Ecological Informatics 76 (2023) 102133

Contents lists available at ScienceDirect

Ecological Informatics

journal homepage: www.elsevier.com/locate/ecolinf

Machine learning models to predict daily actual evapotranspiration of citrus orchards under regulated deficit irrigation

Antonino Pagano [a,c,*], Federico Amato [a], Matteo Ippolito [b], Dario De Caro [b], Daniele Croce [a,c], Antonio Motisi [b], Giuseppe Provenzano [b], Ilenia Tinnirello [a,c]

[a] Department of Engineering, University of Palermo, Viale delle Scienze, Building 9, 90128 Palermo, Italy
[b] Department Agriculture, Food and Forest Sciences, University of Palermo, Viale delle Scienze, Building 4, 90128 Palermo, Italy
[c] CNIT - Consorzio Nazionale Interuniversitario per le Telecomunicazioni, Parma, Italy

ARTICLE INFO

Keywords:
Actual evapotranspiration
Machine learning
Artificial Neural Network
Multi-Layer Perceptron
Random Forest
Citrus orchard
Regulated deficit irrigation

ABSTRACT

Precise estimations of actual evapotranspiration (ET_a) are essential for various environmental issues, including those related to agricultural ecosystem sustainability and water management. Indeed, the increasing demands of agricultural production, coupled with increasingly frequent drought events in many parts of the world, necessitate a more careful evaluation of crop water requirements.

Artificial Intelligence-based models represent a promising alternative to the most common measurement techniques, e.g. using expensive Eddy Covariance (EC) towers. In this context, the main challenges are choosing the best possible model and selecting the most representative features. The objective of this research is to evaluate two different machine learning algorithms, namely Multi-Layer Perceptron (MLP) and Random Forest (RF), to predict daily actual evapotranspiration (ET_a) in a citrus orchard typical of the Mediterranean ecosystem using different feature combinations. With many features available coming from various infield sensors, a thorough analysis was performed to measure feature importance, scatter matrix observations, and Pearson's correlation coefficient calculation, which resulted in the selection of 12 promising feature combinations. The models were calibrated under regulated deficit irrigation (RDI) conditions to estimate ET_a and save irrigation water. On average up to 38.5% water savings were obtained, compared to full irrigation. Moreover, among the different input variables adopted, the soil water content (SWC) feature appears to have a prominent role in the prediction of ET_a. Indeed, the presented results show that by choosing the appropriate input features, the accuracy of the proposed machine learning models remains acceptable even when the number of features is reduced to only 4. The best performance was achieved by the Random Forest method, with seven input features, obtaining a root mean square error (RMSE) and a coefficient of determination (R^2) of 0.39 mm/day and 0.84, respectively. Finally, the results show that the joint use of SWC, weather and satellite data significantly improves the performance of evapotranspiration forecasts compared to models using only meteorological variables.

1. Introduction

According to the recent global report on water use published by UNESCO, irrigation represents about 70% of the global consumption of available freshwater (WWDR, 2021). Therefore, adopting sustainable agriculture is of paramount importance to minimize water consumption. In this context, pushing the agricultural system as a whole toward ecologically sustainable solutions is a major challenge given the increasing insufficiency of water availability (Gangopadhyay et al., 2023). Recent research suggests that farmers should be encouraged to adopt new solutions, particularly in drought-prone regions, in order to optimize both water quantity and quality, and ensure less water consumption for a more environmentally friendly future for the next generations (Lap et al., 2023).

In particular, in the Mediterranean ecosystems, which are characterized by dry and hot summers and rainfall mainly occurring in fall and winter, it is important to adopt sustainable irrigation strategies to increase water use efficiency and preserve water resources. The optimization of irrigation water employment in agriculture can be obtained, from the one hand, by estimating the exact crop water requirement and,

* Corresponding author.
E-mail address: antonino.pagano@community.unipa.it (A. Pagano).

https://doi.org/10.1016/j.ecoinf.2023.102133
Received 6 October 2022; Received in revised form 15 May 2023; Accepted 15 May 2023
Available online 19 May 2023

from the other, through the application of dynamic irrigation strategies, such as the regulated deficit irrigation (RDI). The main goal of these strategies is to save water by controlling in real time the field irrigation as a function of the water status of soil and plants. This can be quantified by means of heterogeneous sensors and data aggregation techniques, in order to identify conditions for reducing the water consumption without affecting the crop growth. For example, it has been proved that RDI can be applied to citrus orchards during the stage II of crop without determining significant impact on crop yield (Castel, 2000; González-Altozano, 2000; Consoli et al., 2014; Stagno et al., 2015; Rallo et al., 2017; Puig-Sirera et al., 2021). However, the application of RDI strategies requires accurate monitoring to avoid severe crop water stress which can produce a decline in yield and/or irreversible effects on crop growth.

From field sensors to water needs. In order to monitor the crop water needs in real-time, several data sources for estimating the field status can be considered, among which meteorological data, soil water contents, drill and drop sensors, satellite images and vegetation indices. Different models for studying the soil water balance (SWB) are then applied for mapping infield data into a precise estimation of the water needs (Kelley et al., 2019). An important parameter for this estimation is the evapotranspiration (ET_a), which is the combination of two distinct processes: water evaporation from the soil surface, E_a and water transpiration from the plant canopy, T_a, depending on the climate and soil water status (Pereira et al., 2020). Recently, several data-driven models (artificial neural networks, K-nearest neighbors, random forest, etc.) have been proposed for predicting evapotranspiration even with a limited amount of infield sensors, i.e. by working only with some low-cost typologies of sensors or with a limited spatial granularity of measurements (Aghajanloo et al., 2013; Granata, 2019; Walls et al., 2020; Yamaç, 2021). Models are customized not only for different climates, but also for different typologies of crops, such as potato crops (Aghajanloo et al., 2013; Yamaç et al., 2020; Talib et al., 2021), green pepper crops (Liu et al., 2020), or cereal crops (Talib et al., 2021; Tang et al., 2018; Abrishami et al., 2019; Han et al., 2021; Hashemi et al., 2020; Elbeltagi et al., 2020). The models can be studied in combination with the irrigation policy, for minimizing the water consumption, as described in Zhang et al. (2016) for the case of a rice crop. However, these works focus on herbaceous crops or horticultures only. Other models for estimating the field water needs are based on the study of the surface energy balance, by processing land surface temperature (LST) (Reyes Rojas et al., 2021). These approaches have been demonstrated in the case of olive and pomegranate orchards and vineyards but, to the best of our knowledge, there is no previous literature focusing on the definition of models for citrus orchards, despite the fact that in the Mediterranean basins citrus is one of the most cultivated crops (MAPA, 2019). Citrus orchards have high water requirements (Rallo et al., 2017; Hari et al., 2010) and differ significantly from olives and pomegranates crops, which are characterized by a high capacity to resist in arid environments (Pierantozzi et al., 2013; Volschenk, 2020).

Reference, potential and actual evapotranspiration. It is important to note that most existing literature employs machine learning (ML) models to predict the crop *reference* evapotranspiration (*ETo*) or potential evapotranspiration (ET_c), whereas the focus of this paper is on *actual* evapotranspiration (ET_a), which plays a key role in the quantitative evaluation of the actual crop water requirements, necessary for irrigation water management. While ET_a values are considered in ecosystem studies, for studying wetland conservation (Granata et al., 2020) and water cycles (Zhang et al., 2021), the comprehensive reviews of evapotranspiration models presented in Krishnashetty et al. (2021), Jing et al. (2019) focus on *ETo* only. In Krishnashetty et al. (2021), which compares several papers from 2009 to 2021, the main goal of *ETo* estimation is developing intelligent irrigation systems, while in Jing et al. (2019) it is demonstrated how *ETo* models developed from 2007 to 2019 can be used for a wide climatic range. Despite the number of proposed models, several issues for the application of these models are still open. In fact, evapotranspiration is a nonlinear and complex phenomenon, and its estimation is based on the availability of several climatic and crop parameters and their mutual interactions with each other. Consequently, the transition from *ETo* to more significant quantities such ET_a is not straightforward. Indeed, while *ETo* can be derived by using only climatic variables, ET_a depends on the specific crop, as well as on soil and plant conditions. Tables 1,2 summarize the main characteristics of related works on potential evapotranspiration and actual evapotranspiration estimation, respectively, by comparing the approach, crop typology, dataset size, number of input features and model accuracy.

Impact of hydrological factors. Recent papers like (Wang et al., 2022; Walls et al., 2020; Wang et al., 2023; Mosre et al., 2021) used ML to study ET_a only from a generic hydrology or atmospheric point of view, and do not consider irrigation strategies like RDI. For example, Izadifar et al. (2010) models ET_a using ANN and Genetic Programming in a Canadian landscape covered by spontaneous vegetation; consequently, the study does not analyze water requirements in a specific crop and does not consider possible irrigation strategies. In Hao et al. (2022) the authors quantified the impact of some hydrological factors on ET_a using Bayesian model averaging for forest, cropland, and grassland ecosystems. In addition, it was demonstrated that soil moisture does not contribute significantly to ET_a in forest areas because vegetative transpiration comprises a large portion of ET_a. Finally, the work in Liu et al. (2020) combines ET_a predictions with RDI, but only for horticulture.

Paper contributions. Taking into account the limitations of current ET_a models, the aim of this work is defining a data-driven model for predicting actual evapotranspiration of a citrus orchard under regulated deficit irrigation. To this purpose, we exploit a large dataset of infield measurements collected in a suburb of Palermo, in Italy, which includes meteorological data, Vegetation Indices (VIs), soil water contents, as well as direct measurements of ET_a (to be used as a ground-truth). A variety of input combinations are explored, analyzing feature importance and Pearson's correlation coefficient, and studying the performance of several ML models (namely, MLP and RF). Interestingly, the presented results show that the accuracy of the proposed ML models remains acceptable even reducing the input features down to four. To the best of our knowledge, we are the first to estimate ET_a in a hot summer Mediterranean ecosystem under RDI, with an average water saving of up to 38.5%, compared to full irrigation management. These estimation models are fundamental to understand and reduce the impact of climate change and water scarcity, thus promoting sustainable agricultural irrigation solutions.

2. Background and motivation

The application of irrigation strategies such as RDI during specific stages of crop growth could result in the optimization of irrigation water use in agricultural ecosystems. The actual crop water requirement can be assessed, among others approaches, by the continuous monitoring of soil water content, as investigated by Lukangu et al. (1999), or using soil water balance (SWB) models (Pereira et al., 2020). In the former, the quality of the results depends on the accuracy and acquisition time of the soil moisture sensors, while the latter requires the accurate estimation of actual crop evapotranspiration, ET_a. Direct measurements of ET_a can be acquired by weighing lysimeters (Schrader et al., 2013), which however are characterized by high installation and maintenance costs. On the other hand, indirect methods to estimate ET_a include the widely used dual crop coefficient approach, suggested in the FAO-56 paper (Allen et al., 1998), and the application of the surface energy balance (SEB), such as the Surface Energy Balance Algorithm for Land (SEBAL) (Bastiaanssen et al., 1998), and Two-Source Energy Balance Model (TSEB) (Norman et al., 1995; Yao et al., 2010). According to the dual crop coefficient approach (Allen et al., 1998) the maximum ET_a can be estimated as the product of crop reference evapotranspiration (ETo) and the term $(K_{cb} + K_e)$, being K_{cb} the basal crop coefficient and K_e the soil evaporation coefficient. The K_{cb} coefficients for the different crops and

Table 1
Literature comparison of models to predict **potential** evapotranspiration (ET_c) considering *RMSE* and R^2.

References	Model	Crop or vegetation	Length of dataset [days]	Number of input features	*RMSE* [mmd^{-1}]	R^2
Elbeltagi et al. (2020)	DNN	Wheat	17531	3	0.15–0,42	0,94–0,97
Yamaç et al. (2020)	kNN, ANN, AdaBoost	Potato	240	1–4	0,24 −1,01	0.68–0.96
Yamaç (2021)	kNN, SVM, RF, AdaBoost	Sugar beet	340	3–7	0,22–1,13	0.79–0.99
Aghajanloo et al. (2013)	ANN, NNGA, MNLR	Potato	990	1–6	0,05–0,35	0.43–0.96
Han et al. (2021)	MLR, BP	Maize, wheat soybean	900	4–5	1,19–1,52	0.69–0.90
Hashemi et al. (2020)	MLP, RBF	Barley	200	4	*NRMSE* 0.23–0.31	0,89–0,93
Abrishami et al. (2019)	ANN	Wheat, maize	250–430	4–8	*NRMSE* 0,10–0.54	0.86–0.99

Notes: RF = Random Forests, SVM = Support Vector Machines, ANN = Artificial Neural Network, MLR = Multiple Linear Regression, kNN = k-nearest neighbors, MLP = Multi-layer Perceptron, AdaBoost = Adaptive Boosting, NNGA = Neural Network–Genetic Algorithm, MNLR = Multivariate Nonlinear Regression, BP = Back-Propagation neural network, DNN = Deep Neural Network, RDF = Radial Basis Functions, NRMSE = Normalized Root Mean Squared Error.

Table 2
Literature comparison of machine learning models to predict **actual** evapotranspiration (ET_a) considering *RMSE* and R^2.

Reference	Models	Crop or vegetation	Length of dataset [day]	Number of input features	*RMSE* [mmd^{-1}]	R^2
Granata (2019)	M5P, BAGGING, RF, SVR	Pastures grass	1825	3–6	0.18–0.40	0.93–0.98
Walls et al. (2020)	ANN	Different land cover	11713	2–5	0.39–0.78	0.98–0.99
Liu et al. (2020)	ENN	Green peppers	800	10	0.35–0.61	0.86–0.97
Talib et al. (2021)	RF, LSTM	Corn, soybeans, potatoes	6208	5–16	0.40–1.30	0.42–0.70
Wang et al. (2022)	LSTM	Grassland, Forest, Alpine meadow	300–500	4–8	0.21–1.06	0.16–0.80
Mosre et al. (2021)	LR - EFS	Grassland, Open shrubland, Barren vegetation	4017	5–18	0.42–1.81	0.15–0.82
Granata et al. (2020)	RF, MLP, kNN, ARDS	Sawgrass	2069	3–7	0.42–1.06	0.42–0.90
Zhang et al. (2021)	RF	Grassland	Datasets of various sizes	21	0.28–0.73	0.64–0.89
Wang et al. (2023)	RF	Different land cover	Datasets of various sizes	7	0.99–2.18	0.32–0.75
Izadifar et al. (2010)	ANN, GP, SAS/STAT	Spontaneous flora	150	5–9	0.06–0.10	R: 0.71–0.88
Hao et al. (2022)	BMA	Grassland, Cropland, Forest	Datasets of various sizes	7	0.32–0.67	R: 0.83–0.97
Present work (2023)	RF, MLP	Citrus orchard	576	4–10	0.39–0.57	0.69–0.84

Notes: M5P = Quinlan's M5 algorithm or M5P regression tree, RF = Random Forests, SVR = Support Vector Regression, ANN = Artificial Neural Network, ENN = Elman Neural Network, LSTM = Long short-term memory, LR = Linear Regression, EFS = Exhaustive Feature Selection, MLP = multilayer perceptron, k-NN = k-nearest neighbors, ARDS = Additive Regression of Decision Stumps, GP = Genetic Programming, SAS/STAT = Statistical model (multiple regression equation), BMA = Bayesian Model Averaging, Cub = Cubist package in R, Sin = sinusoidal models.

stages of vegetative growth, tabulated in the FAO-56 paper (Allen et al., 1998), have been recently updated by Rallo et al. (2021) to account for the research published in the last 20 years. *ETo* represents the atmospheric evaporative demand, whose values can be computed based on air temperature, solar radiation, wind speed and relative air humidity acquired by a standard weather station (Alkaeed et al., 2006). When the soil water content is limiting evapotranspiration, it is necessary to include two additional coefficients, K_s and K_r, with values ranging between 0 and 1, to reduce crop transpiration and soil evaporation, respectively. In a recent review, Pôças et al. (2020) showed the possibility to derive the basal crop coefficient, K_{cb}, based on linear and non-linear relationships employing, as independent variables, vegetation indices (VIs) derived by remote sensing data in the visible and near-infrared domains, whereas earlier, Lei and Yang (2014) proposed to estimate K_{cb} based on a linear function of VIs obtained in the shortwave region.

The SEB models are used to estimate latent heat flux (LE) as the residual term of the energy balance equation. The values of LE measured by the Eddy Covariance (EC) tower have been largely used to assess ET_a. The common configuration of EC towers consists of an infrared open-path gas analyzer to measure H_2O vapor and CO_2 concentration in the atmosphere, a 3D-sonic anemometer to measure the sonic air temperature and the three components of wind speed, a 4-components net radiometer to measure the net radiation and a flux plate to measure the soil heat flux. Although both the water and energy balance models have been largely used to estimate ET_a, the first one requires a large number of meteorological variables to evaluate *ETo* (not always available and with acquisition times not enough adequate for the purpose (Yamaç et al., 2020)), whereas the second, despite the smaller number of required variables, needs the availability of an EC tower equipped with quite expensive instruments. Furthermore, the quality and temporal continuity of the acquisitions can be influenced by the different measurement conditions from the theoretical assumptions, as well as by the malfunction of the instruments caused by the meteorological conditions and also by the imperfect calibrations of the sensors (Masseroni et al., 2014).

The limitations of the classical methods described above indicate the need to assess alternative procedures to increase the availability and accessibility of ET_a measurements. For this reason, ML algorithms can be powerful tools for predicting actual evapotranspiration. Only recently, researchers applied ML to predict two important quantities, ET_c and/or ET_a, which are of paramount interest for crop irrigation management. Indeed, approximately 90% of the papers listed in Tables 1 and 2 have been published within the past four years. Specifically, Table 1 provides a summary of the research using ML models to estimate potential evapotranspiration (ET_c), which is considered a good approximation of ET_a for healthy crops (no diseases) and without water stress. From the table, the ET_c estimation accuracy, measured in terms of *RMSE* and R^2, ranges on average from 0.37 mmd^{-1} to 0.89 mmd^{-1} and between 0.75 and 0.96, respectively. Similarly, Table 2 reports papers focusing on ET_a,

with average ranges of *RMSE* and R^2, from 0.37 mmd^{-1} to 0.97 mmd^{-1} and between 0.55 and 0.86, respectively. However, these results were mostly obtained in forest, cropland and grassland ecosystems, characterized by an homogeneous soil cover condition. Instead, in this paper we focus on the prediction of ET_a in a citrus orchard under regulated deficit irrigation, in a Mediterranean ecosystem. To the best of our knowledge, we are the first to employ machine learning models to predict ET_a in tree orchards.

3. Materials and methods

3.1. Description of the study area and experimental layout

The experiment was carried out for four years (2018–2021) in a citrus orchard (Citrus reticulata Blanco, cv. Mandarino Tardivo di Ciaculli) located in a suburb of Palermo, Italy (38°4' 53.4" N, 13° 25' 8.2" E), as shown in Fig. 1. The field extension is about 0.4 ha, with trees planted at a spacing of 5.0 × 5.0 m and an average height of about 2.5 m. The average fraction cover is about 0.48. The field is generally irrigated with a subsurface drip system, operating from 2018, with two lateral pipes, which contain co-extruded emitters discharging 2.3 l/h at a pressure of 100 kPa with a spacing of 1.0 m (i.e.,10 $emitters/tree$), per plant row, one on each side of the tree, at 1.1 m from the trunks,installed at 0.30 m depth. However, the old micro-sprinklers irrigation system, operating until 2017, is occasionally activated mainly before weeding. The regulated deficit irrigation (RDI) strategy is described in detail in Ippolito et al. (2022). The climate is Mediterranean, with rainfall generally concentrated in fall and winter, and high temperatures in summer. According to the recent version of Köppen climatic classification, the zone has a hot summer Mediterranean climate (Csa) (Kottek et al., 2006). Fig. 2 shows the climatic analysis in terms of cumulative precipitation and crop reference evapotranspiration, as well as the irrigated water volumes, provided to the field. Considering the annual cumulative precipitation, a total of 924 mm was recorded in 2018, and only 551 mm and 577 mm in 2019 and 2020. Furthermore, at the end of November 2021, the cumulative precipitation was equal to 776 mm. On the other hand, the annual crop reference evapotranspiration was 931 mm in 2018, 1069 mm in 2019 and 1076 mm in 2020, as a consequence of the relatively higher daily ETo values registered in 2019 and 2020. Finally, at the end of November 2021, the cumulative crop reference evapotranspiration was equal to 1013 mm. The differences in the cumulative values of irrigation were due to the pluviometric deficit ($P - ETo$) values at the beginning of the irrigation season, equal to 0 mm in 2018, −84 mm in 2019, −243 mm in 2020, and −178 mm in 2021. The applied RDI strategy allowed an average water saving of about 38.5%, in 2018, 2019 and 2020, compared to the full irrigation (FI) management which was followed by the farmer in the rest of the field. The extraordinary high temperatures that were reached during the summer 2021 and the crop conditions before the water stress application period, induced the farmer not to apply the RDI strategy in this year.

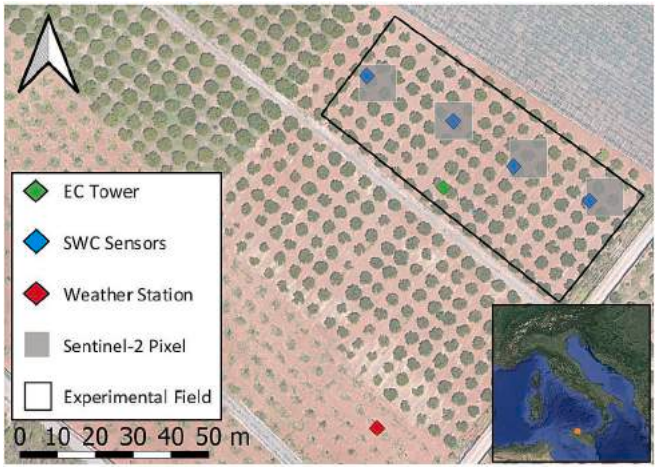

Fig. 1. Map of the experimental site showing the location of the weather station (WD), flux tower (EC), and drill and drop soil water content sensors; the four Sentinel-2 (L2A/L2B) pixels are also shown.

A standard WatchDog 2000 weather station (WS) (Spectrum Technologies, Inc., Aurora, IL, USA) is installed near the field (see Fig. 1)) to collect, every 30 min, the values of air temperature, $T[^\circ C]$, global solar radiation, $R_s[MJm^{-2}d^{-1}]$, relative air humidity, $RH[\%]$, wind speed and direction at 2 m height, $U_2[ms^{-1}]$, and rainfall height, $P[mm]$. Since March 2019, measurements of actual evapotranspiration, $ET_a[mm]$ have been acquired by an Eddy Covariance (EC) flux tower (Fig. 1). The tower is equipped with a 4-components net radiometer (CNR4, Campbell Scientific Inch., Logan, Utah) installed at 3.0 m height, a three-dimensional sonic anemometer (CSAT3-D, Campbell Scientific Inch., Logan, Utah) and an infrared open patch gas analyzer (Li-7500, Licor bioscience inch., Lincoln, Nebraska) to measure, respectively, the net radiation, $Rn[Wm^{-2}]$, with a frequency of 30 min, as well as the 3D-components of wind speed and the concentrations of H_2O vapor and CO_2 in the atmosphere with a frequency of 20 Hz. All the high and low-frequency data are stored in a CR3000 datalogger (Campbell Scientific Inch., Logan, Utah) equipped with a 2 GB memory card. Sensible, $H[Wm^{-2}]$ and latent, $\lambda ET[Wm^{-2}]$ heat fluxes were evaluated as:

$$H = \rho c_p \sigma_{WT} \tag{1}$$

$$\lambda ET = \lambda \sigma_{WQ} \tag{2}$$

where $\rho[g/m^3]$ is the air density, $c_p[Jg^{-1}K^{-1}]$ is the air specific heat capacity at constant pressure, $\sigma_{WT}[mKs^{-1}]$ is the covariance between vertical wind speed and air temperature, $\lambda[Jg^{-1}]$ is the latent heat of vaporization and $\sigma_{WQ}[gm^{-2}s^{-1}]$ is the covariance between vertical wind speed and the water vapour density.

To estimate daily crop reference evapotranspiration, $ETo[mmd^{-1}]$, the FAO-56 Penman–Monteith (PM) equation (Allen et al., 1998) was used:

$$ETo = \frac{0.408\Delta\left(R_n - G\right) + \gamma\left(\frac{900}{T_a} + 273\right)\left(U_2\left(e_s - e_a\right)\right)}{\Delta + \gamma(1 + 0.34U_2)} \tag{3}$$

where $\Delta[kPa/^\circ C]$ is the slope of saturation vapour pressure curve, $R_n[MJm^{-2}d^{-1}]$ is the net radiation at the crop surface, $G[MJm^{-2}d^{-1}]$ is the soil heat flux density, $(e_s - e_a)[kPa]$ is the actual vapour pressure deficit, $\gamma[kPa^\circ C^{-1}]$ is the psychrometric constant and $U_2[ms^{-1}]$ is the wind speed measured thus at 2 m height. When considering the single crop coefficient approach, the values of ET_a can be obtained as:

$$ET_a = (K_c K_s) ETo \tag{4}$$

where ETo is the crop reference evapotranspiration, K_c is the crop coefficient and K_s is the water stress coefficient. The contribution of soil evaporation and crop transpiration is represented by a single K_c accounting for the difference between the reference crop and the considered crop in terms of biophysical characteristics such as canopy properties, ground cover and aerodynamic resistance. The water stress coefficient, K_s, ranging between 0 and 1, is introduced as a multiplicative factor to take into account the actual soil water status. Based on the irrigation strategy adopted in the field, the value of K_s resulted generally equal to 1.0, except during phase II of fruit growth (beginning of July-mid August), when $K_s < 1$ as a consequence of the limited water application.

The dynamic of soil water content (SWC) is monitored by four drill and drop sensors (Sentek Pty Ltd, Stepney, Australia) installed 0.8 m far from the tree trunks, which provide the measurements up to 0.6 m depth (in steps of 0.1 m), with a time resolution of about 30 min. All sensors were interfaced with electronic boards that use license-free

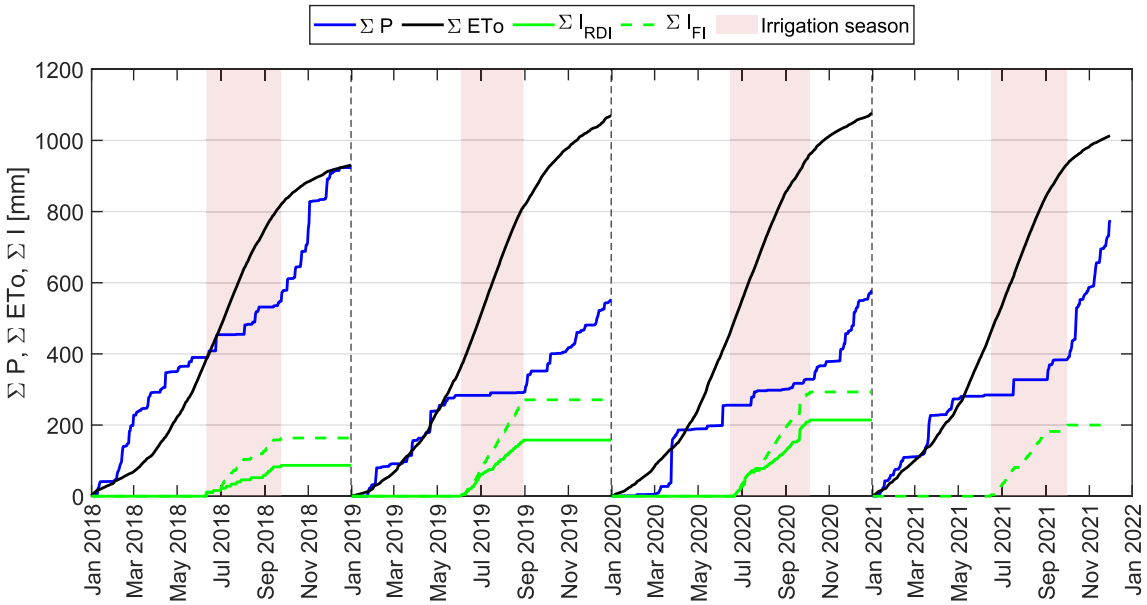

Fig. 2. Cumulative precipitation, Σ*P*, crop reference evapotranspiration, Σ*ETo*, and irrigations, Σ*I*, distributions during 2018–2022. The box indicates the irrigation season.

communication to transmit data to a gateway, which in turn enables Internet connections. The connection is used to log in as a client to a TCP/IP server, which decodes packet transmission and stores the data in a MySQL database.

The Spatio-temporal variability of vegetation indices based on reflectance data in the visible (VIS), near infrared (NIR) and shortwave infrared region (SWIR) of the electromagnetic spectrum was investigated based on the images acquired by Sentinel-2 twin satellites (2A and 2B), characterized by a temporal resolution of about 5 days. In particular, the multi-spectral images (MSI) level 2A provide high-resolution data with spatial resolutions of 10 m, 20 m and 60 m, calibrated in reflectance at the bottom of the atmosphere (BoA), orthorectified and corrected for the atmospheric effects (ESA,https://scihub.copernicus.eu/) (Main-Knorn et al., 2017). The available scenes were used to calculate the normalized difference vegetation index (NDVI) (Rouse et al., 1974; Toosi et al., 2022) and the normalized difference water index (NDWI) (Gao, 1996) as:

$$NDVI = \frac{\rho_{nir} - \rho_{red}}{\rho_{nir} + \rho_{red}} \tag{5}$$

$$NDWI = \frac{\rho_{nir} - \rho_{swir}}{\rho_{nir} + \rho_{swir}} \tag{6}$$

where ρ_{nir}, ρ_{red} and ρ_{swir} are the near-infrared, red and shortwave reflectance, respectively. The corresponding central wavelength, for Sentinel-2A and -2B satellites, are 664.6 nm and 664.9 nm for the red band (B4), 832.8 nm and 832.9 nm for NIR (B8), and 1613.7 nm and 1610.4 nm for SWIR (B11).

3.2. Dataset description and pre-processing

The available database includes weather data recorded by the weather station from January 2018 to November 2021, as well as the micro-meteorological data acquired by the EC tower from March 2019 to November 2021, in both cases registered at sub-hourly time-steps. The former dataset was used to estimate *ETo*, by Eq. (3). The latter dataset was processed, using a specific software developed by Manca (2003), excluding all the records acquired in days where the rainfall height was higher than 2.5 mm. The suitability of the records acquired by the EC tower was assessed based on the energy balance closure quantified by the closure ratio, *CR*, (Prueger et al., 2005), representing the slope of the regression line of the turbulent heat fluxes against available energy, evaluated as:

$$CR = \frac{LE + H}{R_n - G} \tag{7}$$

where *LE* and *H* are the latent and sensible heat fluxes, R_n is the net radiation and *G* is the heat flux into the soil. Sub-hourly data was then aggregated at daily time steps. However, in March 2020 the COVID-19 pandemic lockdown caused the impossibility to visit the field and fix the EC tower, with consequent acquisition failure. Moreover, a single daily value of SWC, representative of the entire field, was calculated as the average of the available data acquired in the layer 0–0.60 m by the four drill and drop probes. Finally, for the four years considered, 251 images, under clear sky conditions, from Sentinel-2 satellite were downloaded and pre-processed using the R library named "sen2r" (Ranghetti et al., 2020). Using Eqs. (5) and (6), for the whole field the vegetation indices were calculated by a specific script implemented in Matlab® R2019b and then exported in QGIS (release 3.4.3) environment to view the maps of NDVI and NDWI. To determine NDWI at the same spatial resolution as NDVI (10 m), the value of a single-pixel reflectance in the SWIR domain (20 m) was associated with the four reflectance values corresponding to the NIR spatial resolution. For both vegetation indices, a single representative value for the entire plot was obtained by averaging the four values calculated in the pixels containing the drill and drop probes. Table 3 summarizes the source and the size of the available dataset for the four investigated years (2018–2021).

Overall, the complete dataset has a length of 1430 days and contains 12 features (U_2, R_s, RH_{min}, RH_{max}, T_{min}, T_{max}, *ETo*, *SWC*, NDVI, NDWI, DOY,

Table 3
Variables used in the analysis and number of records available in the investigated years.

			2018	2019	2020	2021
Instruments	Variable	Units	365	365	366	334
Drill and Drop	SWC	[$cm^3 cm^{-3}$]	355	344	355	320
WatchDog 2000	*ETo*	[mm d^{-1}]	363	365	366	333
EC Tower	ET_a	[mm d^{-1}]	–	193	120	263
Sentinel-2	Images	[–]	44	75	74	58

ET_a), where DOY is the Day Of the Year and the actual evapotranspiration ET_a represents the variable of interest. This feature has 854 missing values, and for this reason, the proposed neural network models are exploited for ET_a predictions and gap-filling. The climate variables and consequently the *ETo* feature have only three missing values in the dataset, while the SWC, and VIs features have 56 and 1179 missing values, respectively, over the four years of observation.

3.3. Machine learning models

This section describes the design and implementation of the examined ML models. As a starting point, four models were initially tested: Linear Regression (LR), Support Vector Machine (SVR), Random Forest (RF), and Multi-Layer Perceptron (MLP). From preliminary results, omitted here for the sake of brevity, only MPL and RF models were selected for their ability to model the nonlinear evapotranspiration phenomena. The models were implemented using the scikit-learn library (Pedregosa et al., 2011), an open-source ML library, for the python programming language. Furthermore, the code developed in this work is released open source to the scientific community (Git Repository, 2023). This will allow repeatability and ease future research efforts in the development of environmentally sustainable irrigation solutions. In the following, an introduction to Artificial Neural Networks (ANNs) and RF algorithms is presented, followed by the description and validation of the proposed MLP-based and RF predictors.

3.3.1. ANNs and Multi-Layer Perceptron

ANNs are a class of powerful ML tools that can be used to solve classification and regression problems. ANNs can be distinguished in two types of architectures, depending on the types of connection between neurons. In the feedback architectures, the presence of connections between neurons of the same layer or between neurons of the previous layer realizes a feedback connection. In the feedforward architectures, the connections between the neurons do not allow feedback between layers, and the signal is transmitted only to the neurons of the next layer.

A widely used feedforward ANN is the Multi-Layer Perceptron (MLP), constituted by one input layer, one or more hidden layers, and a layer of output neurons. The neurons are connected to the ones of the next layer with a certain weight and, in each neuron, the weighted sum of input variables is transformed into an output value through an activation function, defined as:

$$\mathrm{Y} = \psi\left(\sum w_i{}^{*}x_i + b\right) \tag{8}$$

where w_i is the weight, x_i is the neuron input, b is the neuron bias, and ψ is the activation function.

The training of the network is usually done with a backpropagation algorithm, which is divided into two phases. In the first phase (forwarding), controlled inputs are applied to the network, pushing the activation of the input layer neurons. The signal propagates to the next layers, finally reaching the output neurons. The error between the desired output and the obtained result is then calculated for each neuron. In the second phase (backwarding), the error value is propagated backward and the weights of each link are accordingly modified with an optimization method, which aims to minimize the output error. Finally, the network "model selection" is achieved by choosing a set of hyperparameters (i.e. number of hidden layers, number of neurons in each layer, learning rate, solver weight optimization, epoch scale, activation functions, etc.) which characterize the architecture of the MLP model (Sowmya et al., 2020). The best model is selected comparing the performance scores of all possible combinations of hyperparameters.

3.3.2. Random Forest

A Random Forest is a particular classifier/regressor formed by a set of decision trees represented as independent and identically distributed random vectors. This technique is part of ensemble learning that has made significant improvements in learning accuracy for classification and regression tasks (Breiman, 2001). A random subset of the features is chosen at each candidate split during the learning process when using random forests, which employ a modified tree learning algorithm (Ho, 1998). Each decision tree within the RF is constructed and trained from a random subset of the data in the training set. Therefore, the trees do not use the complete set, and at each node the best attribute is chosen from a randomly selected set of attributes (thus, not necessarily the absolute best attribute). For example, given the training dataset (X, Y), with each element $x_i \in X \in R, y_i \in Y \in R$, one can train M different trees on different subsets, chosen randomly with replacement, and then compute the ensemble average:

$$f\left(x\right) = \sum_{m=1}^{M} \frac{1}{M} f_m\left(x\right) \tag{9}$$

where f_m is the m'th tree. This technique is named bagging, which stands for bootstrap aggregating (Breiman, 1996). The basic idea behind bagging is to average models containing errors but approximately unbiased, so as to reduce the variance of an estimated forecast function. Decision trees are ideal candidates for bagging because they can capture complex interaction structures present in the data and, if grown with sufficient depth, have relatively low bias.

Since decision trees are known to be error-prone, they can benefit in important ways from their averaging. In other words, decision trees lower the model variance without raising bias and, thus, this bootstrapping method improves the model's performance. Indeed, while single tree predictions are very sensitive to noise in the training set, an average of several trees reduces this sensitiveness, provided that the trees are uncorrelated. Highly connected trees result from merely training several trees on a single training set. Through the use of various training sets, bootstrap sampling can de-correlate trees. Thus, randomness is a factor that becomes part of the construction of the RFs, and is intended to increase their diversity and thus decrease their correlation. In the case of a regression, the final result returned by the RF is the average of the numerical result by the different decision trees.

3.3.3. Standardization and performance metrics

In this work, the dataset was standardized to reduce the influence of outliers. All features were normalized and scaled so that they have a similar range. In particular, a standard score based on the following equation was used:

$$z = \frac{x - \mu}{\sigma} \tag{10}$$

where x is the real value of the sample, μ is the mean of the population, and σ is the standard deviation. Using the standard score all features have a zero mean and a unit variance.

The model performance was evaluated based on three statistical indicators: coefficient of determination (R^2), root mean square error (*RMSE*), and mean bias error (*MBE*), calculated according to the following equations:

$$R^2 = 1 - \frac{\sum_{i=1}^{n}\left(y_i - \widehat{y}_i\right)^2}{\sum_{i=1}^{n}\left(y_i - \overline{y}_i\right)^2} \tag{11}$$

$$RMSE = \sqrt{\frac{\sum_{i=1}^{n}\left(y_i - \widehat{y}_i\right)^2}{n}} \tag{12}$$

$$MBE = \frac{\sum_{i=1}^{n}\left(y_i - \widehat{y}_i\right)}{n} \tag{13}$$

where y_i represents the measured evapotranspiration ET_a value of the i-th sample, $\hat{y}_i$ is the corresponding predicted value, and $\bar{y}_i$ is the mean measured data for a total n observations.

3.3.4. Model hyperparameters selection

For both MLP and RF predictors, the grid search technique was applied to compute the optimum values of hyperparameters. Regarding the MLP, the network was implemented with an input layer, 3 hidden layers, and an output layer. In the model selection phase, the performance obtained using different hyperparameters was compared. Specifically, the following hyperparameters were tested:

1. Solvers: Limited-Broyden–Fletcher–Goldfarb–Shanno (L-BFGS), Adam, Stochastic Gradient Descent (SGD) with constant learning rate, SGD with adaptive learning rate;
2. Number of neurons in the hidden layers: from 1 to 100;
3. Regularization factor "alpha" (L2 penalty): $10^{-1}, 10^{-2}, 10^{-3}, 10^{-4}$;
4. Activation function: identity, logistic, tanh, ReLU;
5. Learning Rate: constant, invscaling, adaptive.

The following configuration optimized the performance of the model and was accordingly adopted for analysis: Adam solver (Kingma and Ba, 2014), 10 neurons per hidden layer, alpha $= 10^{-4}$, constant learning rate, and rectifier activation function, also called Rectified Linear Unit (ReLU) activation function, defined as:

$$\mathrm{ReLU}\left(\mathrm{k}\right) = \begin{cases} \mathrm{k}, \text{ if } \mathrm{k} > 0; \\ 0, \text{ if } \mathrm{k} \leqslant 0. \end{cases} \tag{14}$$

In the case of the RF, the hyperparameters include the number of decision trees in the forest, the maximum depth of the decision tree, the number of features considered by each tree when splitting a node, etc. This set of hyperparameters was tested using the grid configuration shown below:

1. Number of decision trees: from 100 to 1000 (in steps of 100);
2. Number of features to consider at every split (max_features): *auto*, *sqrt*, *log2*, *None*;
3. Maximum number of levels in decision tree: None, or from 10 to 100 (in steps of 10);
4. Minimum number of samples required to split a node (samples_split): 2, 5, 10;
5. Minimum number of samples required at each leaf node (samples_leaf): 1, 2, 4;
6. Method of selecting samples for training each tree (bootstrap): True or False;
7. Parameter for minimal cost-complexity pruning (cpp_alpha): from 0 to 0.06 (in steps of $4{\cdot}10^{-4}$).

The following setup was chosen for investigation since it achieved the best prediction accuracy: 1000 trees, max_features = auto, 50 levels, samples_split = 2, samples_leaf = 2, bootstrap = True, cpp_alpha = 0.

Finally, feature analysis was performed to test different combinations of the input features among a set of 12 different possibilities. Moreover, ML algorithms were also exploited to compensate for missing values in the dataset, as detailed in the following Section 3.3.5.

3.3.5. Prediction algorithms and gap filling

This work exploits ML models also to perform gap-filling procedures of missing data. Gaps are present in the VIs because samples are not available with the same time resolution of the other variables. Few data samples were absent in other input features as well (*SWC*, *ETo*, and climate data), as detailed in Section 3.2. Thus, for the missing input data described earlier, the KNN-Imputer was utilized to fill in missing values using the k-Nearest Neighbor approach (Troyanskaya et al., 2001; Thirukumaran and Sumathi, 2012). However, when the number of missing values is greater than the number of observed ones (the case of VIs), iterative imputation was used (Richman et al., 2009). Note also that the dataset misses several ET_a measurements, with 542 complete records out of a total number of 1430 records. Being ET_a the output of the proposed data-driven models, the previous approaches for filling in the missing data were not used. Nevertheless, MLP and RF models were trained only on the sub-set of complete data and the best models can be selected as detailed in the next section. Cross-validation was also used to assess models reliability and avoid over-fitting. Obviously, the trained models can be used for future predictions, as well as for predicting the missing ET_a values of the dataset.

4. Feature analysis and results

For the four years of observation, Fig. 3 (a-d) presents the temporal dynamics of the daily weather variables acquired by the weather station. The annual pattern of daily solar radiation, R_s, is similar across the four years, with maximums values generally slightly lower than 30 $MJm^{-2}d^{-1}$ in summer and minimums lower than 10 $MJm^{-2}d^{-1}$ in winter. The annual dynamic of air temperature, T, follows that of R_s, with the maximum ranging between approximately 13 and 40 $^{\circ}C$ and minimums ranging between 1 and 25 $^{\circ}C$, respectively in winter and summer. The average relative air humidity ranged between 48.0 and 92.4%, whereas wind speed typically remained lower than 2 ms^{-1}, even though some daily peaks of about 4 ms^{-1}or higher were also recorded.

The temporal dynamic of daily air temperature, net radiation and wind speed, as well as the frequency of wind direction recorded by the EC tower in 2019 and 2021 are shown in Fig. 4 (a–d). Compared to the values registered by the weather station, the EC tower slightly underestimated the minimum sonic air temperature and slightly overestimated the maximum sonic air temperature, mainly in summer when the values consistently exceeded 30 $^{\circ}C$. The sonic wind speed was generally higher than the corresponding measurements taken by the cup anemometer installed in the weather station, due to the different installation heights and to the greater sensitivity of the CSAT3-D sonic anemometer. The dominant wind speed resulted in $1.7ms^{-1}$ along the direction of 45° (NE). Fig. 5 (a–c) shows the relationships between the turbulent heat fluxes, $H + LE$, and the available energy, $Rn - G$, measured by the EC tower in 2019, 2020 and 2021. The slope of the regression line, which represents the closure ratio (CR), resulted equal to 0.98 for 2019, 0.88 for 2020 and 1.03 for 2021, indicating the suitability of the estimated energy balance components (Kustas et al., 1999; Er-Raki et al., 2009).

The temporal dynamics of daily crop reference evapotranspiration, *ETo*, actual evapotranspiration, ET_a, and precipitation, P, are depicted in Fig. 6. The annual dynamic of *ETo* follows that of air temperature and global solar radiation, with annual values ranging between about 1 mmd^{-1} in winter and 6 mmd^{-1} in summer; the peak of 8.8 mmd^{-1} registered on May 14, 2020, was due to the simultaneous occurrence of high air temperature, relatively low minimum relative air humidity and high wind speed. The values of ET_a in the considered period were generally lower than daily *ETo*, although they resulted occasionally higher during or immediately after rainy days, as a consequence of the relatively greater contribution of evaporation from soil and/or leaf surface. For this reason, the values of ET_a recorded on days characterized by rainfall heights higher than 2.5 mm were not included for further analysis.

Fig. 7 illustrates the temporal dynamics of daily soil water contents (SWC) obtained by averaging the values acquired by the four probes from the soil surface up to 0.6 m depth. The bottom of Fig. 7 also shows the daily SWC profile. As can be observed, for the four years considered, the average SWC ranged from 0.18 cm^3cm^{-3} to 0.34 cm^3cm^{-3}. The temporal dynamic of SWC is affected by the occurrence of rain events which determines the rapid increase of soil water contents. However, the rise of SWC observed in February, May and June 2020 was

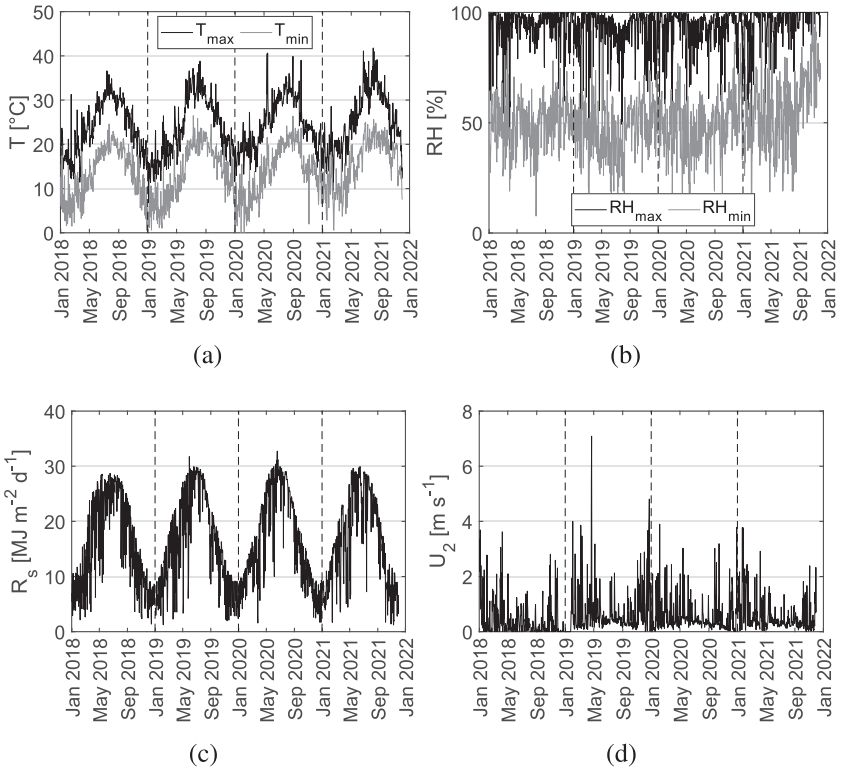

Fig. 3. Temporal dynamic of daily climatic variables registered between 2018 and 2021: a) maximum and minimum air temperatures, b) maximum and minimum relative air humidity, c) global solar radiation and d) wind speed.

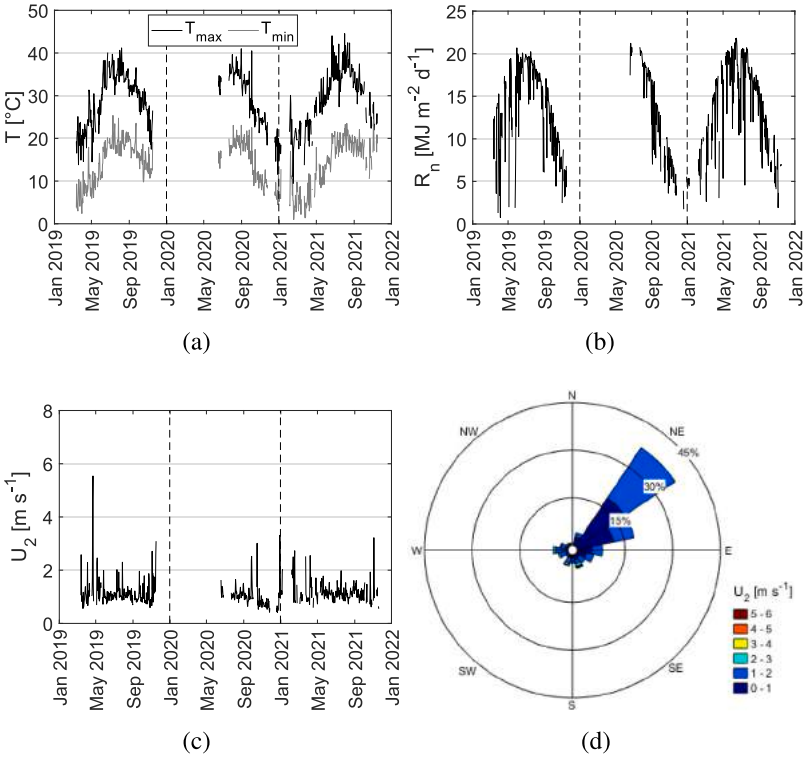

Fig. 4. Temporal dynamic of a) maximum and minimum air temperatures, b) net radiation, c) wind speed and d) frequency of wind direction as registered by the EC tower in 2019, 2020, and 2021.

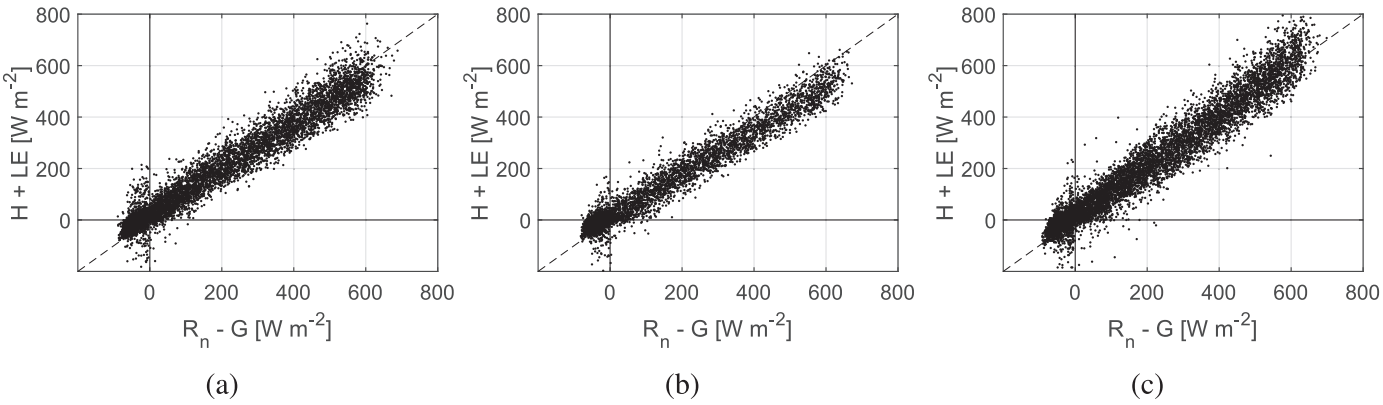

Fig. 5. Relationships between turbulent heat fluxes, H + LE, and available energy, Rn-G, measured by the EC tower for 2019 (a), 2020 (b), and 2021 (c).

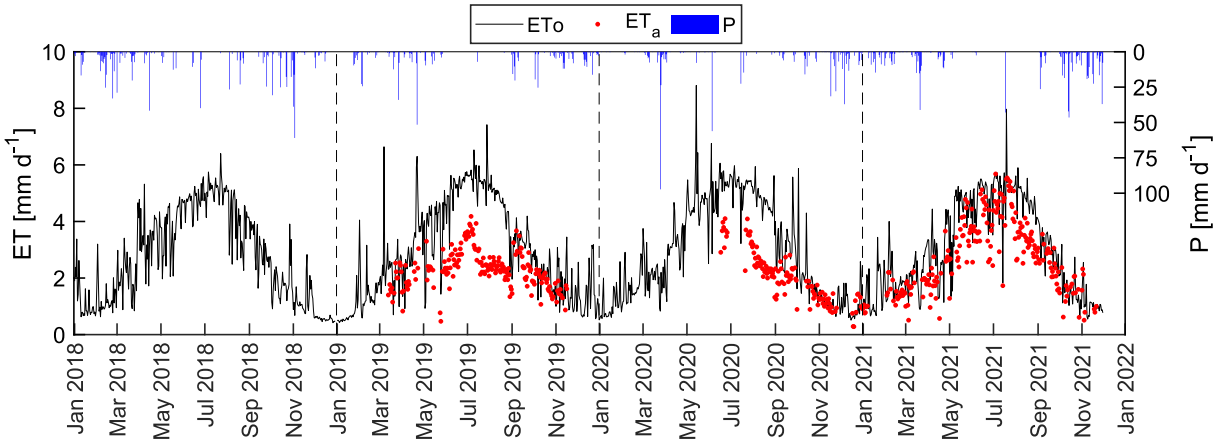

Fig. 6. Temporal dynamic of crop reference evapotranspiration, *ETo*, actual crop evapotranspiration, ET_a, and precipitation, *P*.

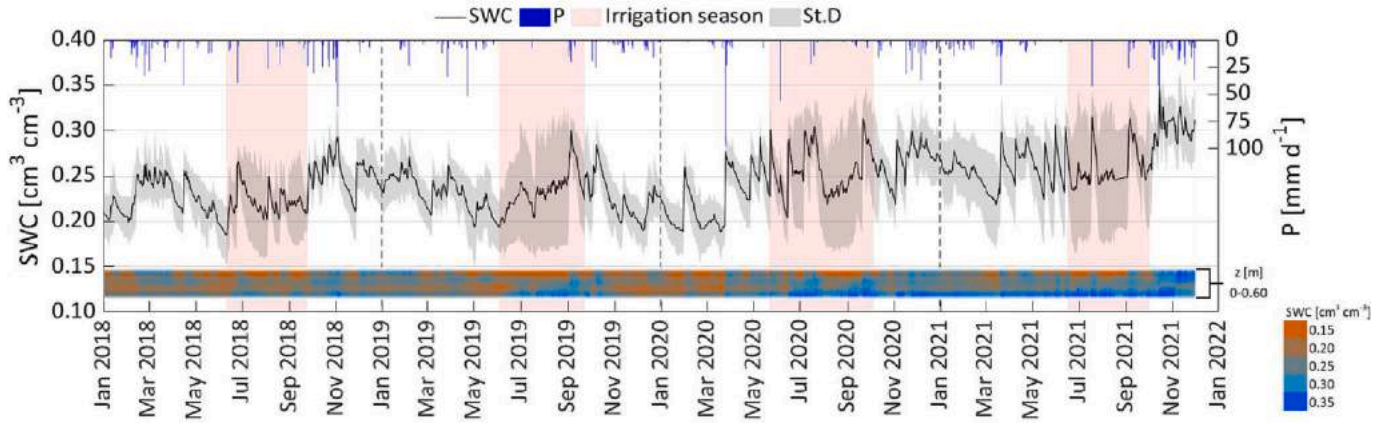

Fig. 7. Temporal dynamics of daily average soil water content, SWC, valid for the entire field and precipitation, P. The pattern of the average SWC profile from 0 to 0.60 m depth is also shown at the bottom of the figure. The box indicates the irrigation season.

associated with wetting events of the upper soil surface operated by the micro-sprinklers irrigation system after long drought periods. The standard deviation associated with daily SWC in February, May and June 2020 as well as in April, May and June 2021 ranged between 0.01 cm^3cm^{-3} and 0.08 cm^3cm^{-3}, with the relatively higher values obtained during the irrigation seasons (from mid of May to the end of September), when the values of SWC at 30–50 *cm* depths resulted considerably higher than those of the upper soil layers, not wetted by the subsurface drip irrigation system.

The temporal dynamic of the average NDVI and NDWI for the four years, illustrated in Fig. 8, shows quite similar patterns. The values of NDVI ranged from 0.40 to 0.90, while the values of NDWI resulted variable between 0.01 and 0.60. Both VIs resulted maximum in winter ($NDVI_{mean} = 0.90, NDWI_{mean} = 0.36$) and minimum during summer ($NDVI_{mean} = 0.59, NDWI_{mean} = 0.10$), with quite low standard deviations as a consequence of the limited variability in the spectral response of the field surface.

4.1. Feature analysis

Since ML models usually portray the relationship between input and output features, a preliminary feature analysis was performed. Indeed, this analysis plays a key role in reducing the dimensionality of the problem by favoring the application of ML models with a limited number of features, reducing the complexity, implementation and deployment costs in the field.

For example, the matrix in Fig. 9 shows at a glance the relationship between each two features: the scatter plot at row n and column m shows the n-th feature as a function of the m-th feature. This is helpful to spot correlations in the dataset, since the more sparse are points in a plot, the more uncorrelated are the two corresponding features. In particular, it is clear that ETo and R_S have a higher correlation with ET_a than other features. Finally, the plots in the diagonal represent the kernel density estimation of each feature, which is an estimate of their probability density function.

Fig. 10 shows the Pearson correlation coefficient, which measures the linear correlation of each couple of features. It ranges between 1 (dark red) and −1 (dark blue), were darker colors indicate higher absolute values, i.e. the two features are strongly correlated (the sign of the coefficient reflects the slope of the linear relation). In this case, the actual evapotranspiration ET_a has a positive Pearson correlation coefficient with the following features: $ETo, R_s, T_{max}, T_{min}$, with a value of 0.8, 0.78, 0.59, 0.38, respectively. On the other hand, the features $NDVI$, $NDWI$, show a strong negative Pearson correlation coefficient with ET_a.

Fig. 11(a) shows the feature importance scores (FIS) of each variable in the dataset for the prediction of ET_a. The higher the FIS, the more important the feature. The importance of a feature is computed as the (normalized) total reduction of the criterion brought by that feature and is also known as the Gini importance (Ravindran et al., 2021). In this work, FIS is computed using the Gradient Boosting Regressor (Kadiyala and Kumar, 2018). Among all features in the dataset, the three most important ones are ETo, SWC, and R_s, with a FIS of 0.577, 0.197, and 0.078, respectively. Note that this result includes the reference evapotranspiration ETo in the input feature analysis. However, since ETo is a climate dependent parameter calculated from other measured climate variables, it is interesting to investigate how FIS changes when ETo is excluded from the dataset. Indeed, from Fig. 11(b), it is clear that excluding ETo from the dataset sharply increases the FIS of R_s from 0.078 to 0.556 compared to the previous feature analysis. In this case, the most important features become R_s, SWC, and DOY.

4.2. Performance evaluation and results

Based on the feature analysis, it was possible to choose the features contained in the entire dataset or eliminate some less relevant features that could compromise the generalization of the model, focusing the attention to the most relevant ones. More into details, Table 4 shows the input feature combinations used to implement the developed models. In particular, for both MLP and RF, combination 1 contains all available features except ETo. From combination 2 to 7 other features with less importance are gradually removed, while combination 8 uses only the variables measured by the weather station. Finally, combinations 9 and 10 do not use the weather variables, but consider the ETo feature instead, and combinations 11 and 12 are the same of models 9 and 10, except that ETo is substituted by R_s, which is the most important feature among weather variables, both in terms of Pearson correlation coefficient and feature importance score.

The results obtained by the different models in terms of RMSE, R^2, and MBE are detailed in Table 5. Specifically, the table shows that both the MLP and RF models perform well, although generally, RF performed better than MLP independently of the input features considered in the model. In particular, the Multi-Layer Perceptron method showed that models MLP1 and MLP5 were the best choices for ET_a estimation, with the lowest RMSE (0.44 mmd^{-1}) and highest R^2 (0.82) score compared to the other input feature combinations. On the other hand, the best scores for the Random Forest predictor are obtained with models RF2, RF3 and RF4, showing an RMSE of 0.39 mmd^{-1} and an R^2 of 0.84. Moreover, low MBE values indicate that ET_a predictions do not deviate much from the corresponding measured values (for all scenarios examined, MBE was between −0.025 and 0.041 mmd^{-1}). Note that, in some cases, a reduction in the number of feature produces equal or even better performances than models including all available features. For example, in the case of the MLP predictor, MLP1 and MLP5 show the same performance, but MLP1 used all the ten features available while MLP5 used only six features (the four less important features were removed, i.e. RH_{min}, RH_{max}, T_{min}, $NDVI$). Similarly, for the RF predictor, performance improved after removing features RH_{min}, T_{min}, and $NDVI$ (i.e. moving from RF1 to RF4). Finally, the RF predictor is also consistent with the reduction of input features: for example, in RF6 and RF11, i.e. using only five features, the RF predictor shows very good scores ($R^2 = 0.82$ and $RMSE = 0.42 mmd^{-1}$, close to the best ones), where RF6 used the first five features with the highest feature importance score ($R_s, U_2, T_{max}, SWC, DOY$), while RF11 used only weather variable R_s and features $SWC, NDVI, NDWI, DOY$. Indeed, from Table 5 it is clear that the joint use of SWC, NDVI, NDWI, and DOY features with ETo (MLP9 or RF9) improves the performance of ET_a predictions compared to models using only weather variables (MLP8 or RF8).

The accuracy of the different models was explored by analyzing the violin plots shown in Fig. 12. These plots show the relative error distributions of all MLP and RF models during irrigation seasons. In the middle of each violin plot, there is a small box plot, with the rectangle representing the ends of the first and third quartiles, and a central white dot for the median. The concentration of the relative error is close to zero, highlighting the good performance of the analyzed models. In particular, Fig. 12(a) shows that the errors of most MLP models (MLP1 to MLP11) have a median greater than zero (in the range $[0.002, 0.076]$%), which means that these models slightly overestimated the ET_a values. Only the MLP12 model had a median error below zero (-0.031%). Fig. 12(b), instead, shows that most of the RF models (9 out of 12) slightly underestimated the ET_a values, with a negative median error (the worst case was RF12, with −0.019%). On the other hand, RF7, RF10, and RF11 had a median above zero (0.004%, 0.044%, and 0.030%, respectively), therefore overestimating ET_a. Finally, the violin plots show that using features set 9 and 10 both MLP and RF had a longer upper tails, indicating that in some occasions these models provided larger overestimates. In addition, the relative error distribution was asymmetrical (positive skew) for most of the considered models. As expected, the RF models had a median error closer to zero, compared to MLP models.

Figs. 13 and 14 show a comparison between observed and predicted ET_a values for the MLP and RF models, respectively, considering all 12 input feature combinations. The figures also show the linear robust regression interpolation forced through the origin (blue line) and the identity line (red dashed), from which it is clear that most of the models have a tendency to slightly underestimate the measured actual evapotranspiration values when $ET_a > 4.5 mmd^{-1}$. On the other hand, a slight overestimation is present for $ET_a < 1 mmd^{-1}$. This behavior based on the ET_a values to be predicted was also noted by Granata et al. (2020). Overall, the slope of the regression line for MLP models ranges between 0.951 and 1.031, while, for RF models, the slope varies between 0.941 and 1.005, which means that the latter have slightly less variance than the former. The slope closest to 1.0 for MLP were observed for the models MLP2 (Fig. 13(b)), MLP7 (Fig. 13(g)), and MLP9 (Fig. 13(i)) characterized by regression slope of 0.992, 1.009, and 1.003 respectively. On the other hand, the best slopes of RF models had values of 1.006, 0.992, and 1.005, for RF1 (Fig. 14(a)), RF4 (Fig. 14(d)), and RF9 (Fig. 14(i)), respectively.

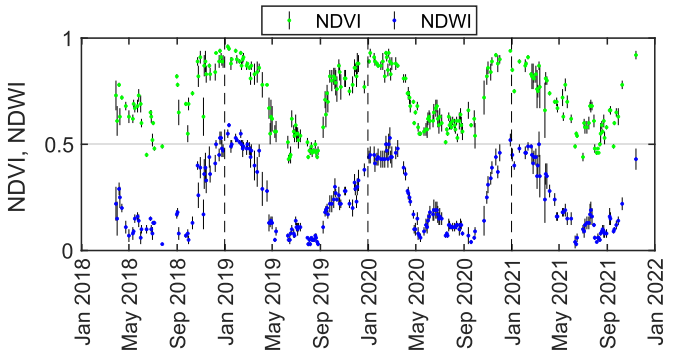

Fig. 8. Temporal dynamics of average NDVI and NDWI with the corresponding standard deviation.

5. Discussion

The results presented in this work suggest that in general both the MLP and RF models were able to accurately describe the nonlinear relationships between weather and crop parameters, providing accurate predictions of ET_a under regulated deficit irrigation. These ML models could be used to optimize irrigation strategies according to the availability of water resources as well as to adopt RDI strategies, saving up to 38.5%, compared to full irrigation management. Therefore, this work offers a contribution to the creation of a sustainable agricultural environment, according to recent work in Gangopadhyay et al. (2023). Moreover, since direct measurements of the actual values of ET_a (e.g. by means of EC towers) can be expensive and complex, in this work we use these values only for training a field-specific data model. Then, the models are used to provide a prediction of ET_a for the examined ecosystem based on low-cost sensor data only, with little impact on estimation accuracy. The results obtained by the models used in this work are summarized in the last row of Table 2. Indeed, the results were generally consistent with the performance of previous studies in the literature when taking into account the average ranges of *RMSE* and R^2 ([0.37, 0.97] mmd^{-1} and [0.55, 0.86], respectively), while the performance of the proposed models varied between 0.39 mmd^{-1} and 0.57 mmd^{-1} for *RMSE* and between 0.69 and 0.84 for R^2.

Furthermore, many of the papers listed in Table 2 estimate ET_a in forest, cropland and grassland ecosystems, characterized by a homogeneous soil cover condition. However, in these scenarios, ET_a is rarely affected by the evaporative processes from the soil (Yao et al., 2010; Hao et al., 2022). Recently the possibility to estimate ET_a in tree crops, through ML models, was assessed by Reyes Rojas et al. (2021), using LST

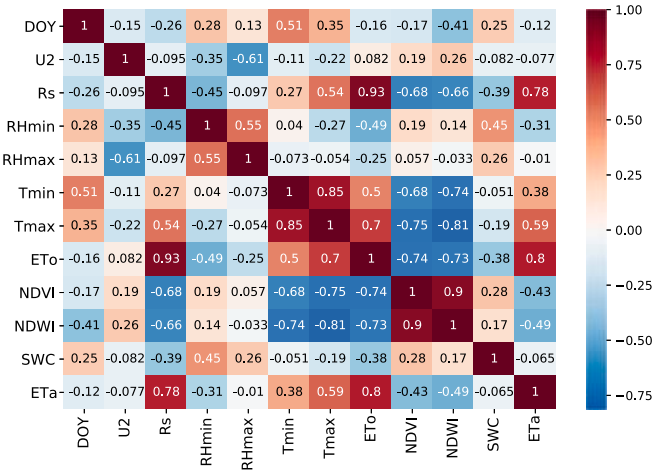

Fig. 10. Pearson correlation coefficient between each pair of features.

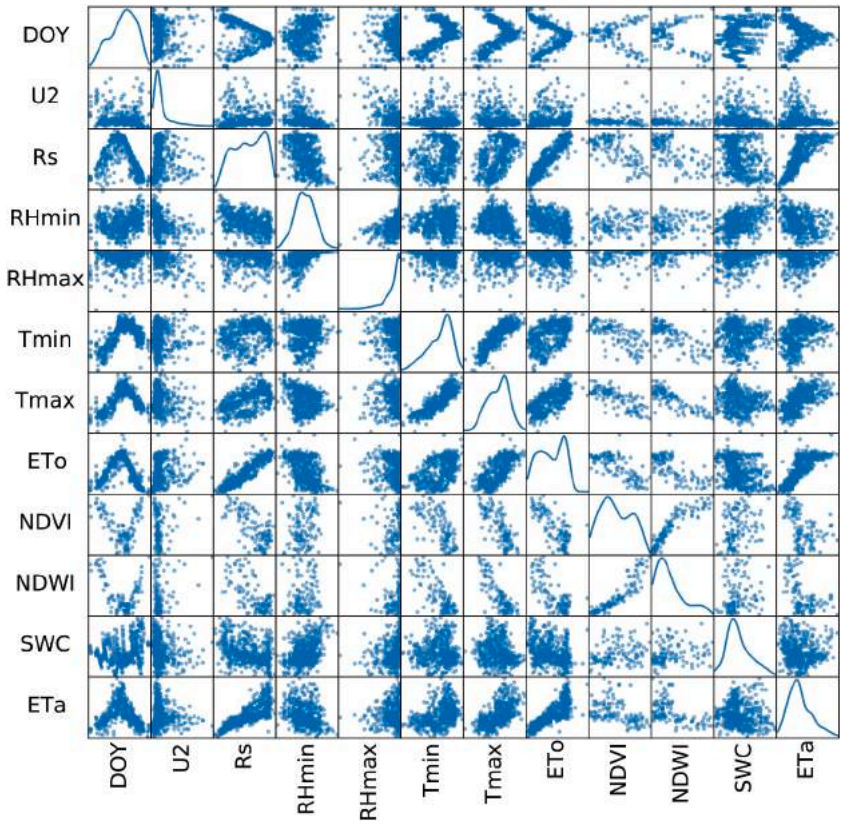

Fig. 9. Scatter matrix used for overview and features analysis in ML models implementation.

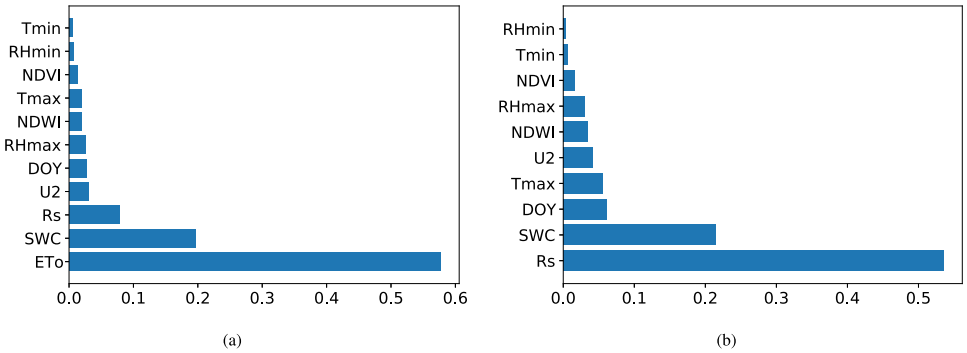

Fig. 11. Feature importance score (FIS) of each feature of the dataset in the ET_a prediction (a), FIS when ETo is excluded from the dataset (b).

as input with a spatial resolution of 10 m, obtained from the downscaling of Landsat-8 LST data, by means of two different models (cubist and RF). In particular, the authors estimated ET_a through the Operational Simplified Surface Energy Balance Model (SSEBop) of olives and pomegranates tree crops, obtaining results slightly worse than the ones presented in this paper. However, it is important to highlight that the ET_a predictions presented in Reyes Rojas et al. (2021) are derived from the application of the SSEBop model and not from an ML model trained using ET_a in situ measurements. Furthermore, the olives and pomegranates crops are characterized by a high capacity to resist arid environments (Pierantozzi et al., 2013; Volschenk, 2020), while citrus orchards are characterized by higher water requirements (Rallo et al., 2017). In this sense, it is possible to affirm that this work represents the first attempt to exploit ML models to predict ET_a in a tree crop under RDI, where nonlinear processes, such as transpiration from the canopy and evaporation from the soil, must be taken into account.

It is important to note that the results obtained in this work are best when the SWC feature is included in the input variables. Indeed, from the results shown in Table 5 and the feature importance analysis (Fig. 11 (a) and (b)), it is clear that SWC has a significant impact on the ET_a prediction. This evidence is supported by other studies in the literature showing that soil moisture becomes a significant factor for modeling ET_a when soil water supply is insufficient (Wang and Liang, 2008; Mosre et al., 2021; Wang et al., 2022; Granata, 2019). Moreover, other works in ecological fields (Girardello et al., 2010; Srinet et al., 2019; Piccioni et al., 2022) confirmed that RF models are able to capture nonlinear dependencies among different variables, supporting the results presented in Table 5 and Fig. 12, in which the RF models appear to best predict the nonlinear phenomena of ET_a.

Finally, other hydrological features such as precipitation (P) and irrigation (I) were also considered as inputs to our ML models. However, these variables were eventually excluded for the following reasons. First, precipitation values are localized measurements and could limit the possibility of generalizing the obtained ML models, as discussed in Mosre et al. (2021), Han et al. (2021). Second, in presence of subsurface drip irrigation systems, irrigation times are weakly correlated with the ET_a measurements (the obtained Pearson correlation and feature importance score were 0.150 and 0.003, respectively). This can be due to both negligible soil surface moisture during the irrigation season and failure to capture flows through the root zone, as explained for example in Talib et al. (2021). Note that, the two variables P and I are indirectly contained in the SWC feature used in our models. In particular, the SWC values were averaged considering four different positions in the field and six different measurement depths, from the surface down to 0.6 m depth. These measurements are thus more accurate for modeling ET_a under deficit irrigation.

Table 4
Input features combination used in input for the MLP and RF models.

Nr.	Input features selected
1	$R_s, U_2, RH_{min}, RH_{max}, T_{min}, T_{max}, SWC, NDVI, NDWI, DOY$
2	$R_s, U_2, RH_{max}, T_{min}, T_{max}, SWC, NDVI, NDWI, DOY$
3	$R_s, U_2, RH_{max}, T_{max}, SWC, NDVI, NDWI, DOY$
4	$R_s, U_2, RH_{max}, T_{max}, SWC, NDWI, DOY$
5	$R_s, U_2, T_{max}, SWC, NDWI, DOY$
6	$R_s, U_2, T_{max}, SWC, DOY$
7	R_s, T_{max}, SWC, DOY
8	$R_s, U_2, RH_{min}, RH_{max}, T_{min}, T_{max}$
9	$ETo, SWC, NDVI, NDWI, DOY$
10	$ETo, NDVI, NDWI, DOY$
11	$R_s, SWC, NDVI, NDWI, DOY$
12	$R_s, NDVI, NDWI, DOY$

6. Conclusions

This work explored the possibility of using ML models for accurately predicting actual evapotranspiration values in Mediterranean citrus orchards, where an RDI strategy is applied. Evapotranspiration data is very relevant to increase the ecosystems resilience, including the sustainability of the irrigation process. Different choices are possible for retrieving this data: deploying the instrumentation devised to perform direct measurements of ET_a (e.g. EC towers) or using this instrumentation only temporarily for training a field-specific data model, which will be able to provide an indirect estimation of ET_a for the examined ecosystem, based on sensors data only.

Since measuring the actual values by means of EC towers can be expensive and complex, the objective of this research was to assess the second choice and study the impact of different features and ML approaches (namely, MLP and RF) on estimation accuracy. To identify the most relevant input data, an in-depth analysis of feature importance and correlation was performed on a dataset based on extensive in-field measurements collected in a suburb of Palermo, in Italy. The dataset includes meteorological data, vegetation indices, soil water contents, as well as direct measurements of ET_a (to be used as a ground-truth), acquired respectively by means of a weather station, satellite images, drill and drop sensors, and an EC tower. The results obtained are promising: data-driven models can achieve an accuracy higher than 82% for predicting ET_a values, especially in the case of RF models.

Moreover, reducing the number of input features from 10 to 5 does not harm the prediction accuracy significantly, thus enabling the possibility of opportunistically selecting in-field sensors. In general, the experiments demonstrated that ET_a is better predicted with agro-meteorological data of high importance (R_s, T_{max}, SWC) combined with vegetation indices, compared to models using weather variables only (i.e. $R_s, U_2, RH_{min}, RH_{max}, T_{min}, T_{max}$). Indeed, both soil water content and solar radiation were significant factors to predict ET_a accurately.

Results show that the prediction of ET_a in a tree crop under RDI strategy, allows an average water saving up to 38.5%, compared to full irrigation, reducing the impact of climate change and water scarcity in the global environmental equilibrium. Furthermore, the approaches proposed in this study, extended to different crops and climate condi-

Table 5
Results and model comparison.

Predictor	Model name	Nr. of input features	Input features	R^2	$RMSE\,[mmd^{-1}]$	$MBE\,[mmd^{-1}]$
Multi Layer Perceptron (MLP)	MLP1	10	$R_s, U_2, RH_{min}, RH_{max}, T_{min}, T_{max}, SWC, NDVI, NDWI, DOY$	0.82	0.44	0.017
	MLP2	9	$R_s, U_2, RH_{max}, T_{min}, T_{max}, SWC, NDVI, NDWI, DOY$	0.80	0.45	−0.025
	MLP3	8	$R_s, U_2, RH_{max}, T_{max}, SWC, NDVI, NDWI, DOY$	0.80	0.46	−0.024
	MLP4	7	$R_s, U_2, RH_{max}, T_{max}, SWC, NDWI, DOY$	0.81	0.44	0.008
	MLP5	6	$R_s, U_2, T_{max}, SWC, NDWI, DOY$	0.82	0.44	0.005
	MLP6	5	$R_s, U_2, T_{max}, SWC, DOY$	0.78	0.47	0.015
	MLP7	4	R_s, T_{max}, SWC, DOY	0.78	0.48	−0.016
	MLP8	6	$R_s, U_2, RH_{min}, RH_{max}, T_{min}, T_{max}$	0.69	0.57	0.001
	MLP9	5	$ETo, SWC, NDVI, NDWI, DOY$	0.75	0.50	−0.002
	MLP10	4	$ETo, NDVI, NDWI, DOY$	0.70	0.56	−0.009
	MLP11	5	$R_s, SWC, NDVI, NDWI, DOY$	0.74	0.53	0.041
	MLP12	4	$R_s, NDVI, NDWI, DOY$	0.72	0.54	0.001
Random Forest (RF)	RF1	10	$R_s, U_2, RH_{min}, RH_{max}, T_{min}, T_{max}, SWC, NDVI, NDWI, DOY$	0.83	0.40	0.013
	RF2	9	$R_s, U_2, RH_{max}, T_{min}, T_{max}, SWC, NDVI, NDWI, DOY$	0.84	0.39	0.011
	RF3	8	$R_s, U_2, RH_{max}, T_{max}, SWC, NDVI, NDWI, DOY$	0.84	0.39	0.009
	RF4	7	$R_s, U_2, RH_{max}, T_{max}, SWC, NDWI, DOY$	0.84	0.39	0.007
	RF5	6	$R_s, U_2, T_{max}, SWC, NDWI, DOY$	0.83	0.40	0.008
	RF6	5	$R_s, U_2, T_{max}, SWC, DOY$	0.82	0.41	0.008
	RF7	4	R_s, T_{max}, SWC, DOY	0.81	0.42	−0.005
	RF8	6	$R_s, U_2, RH_{min}, RH_{max}, T_{min}, T_{max}$	0.72	0.52	0.004
	RF9	5	$ETo, SWC, NDVI, NDWI, DOY$	0.80	0.42	−0.003
	RF10	4	$ETo, NDVI, NDWI, DOY$	0.72	0.52	−0.012
	RF11	5	$R_s, SWC, NDVI, NDWI, DOY$	0.82	0.42	−0.004
	RF12	4	$R_s, NDVI, NDWI, DOY$	0.76	0.48	0.005

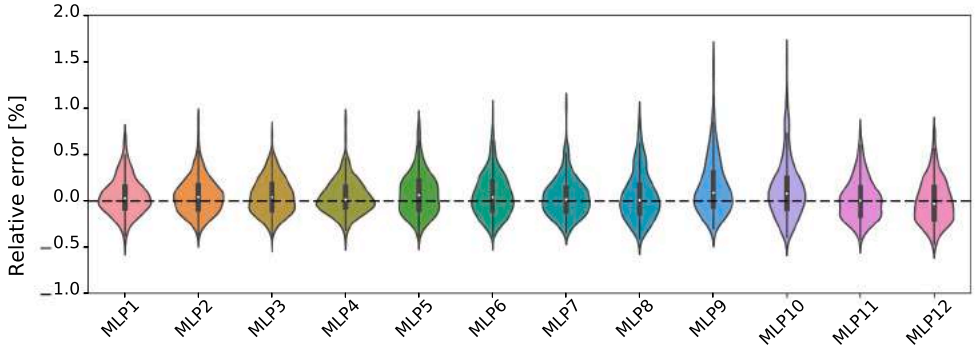

(a) MLP models

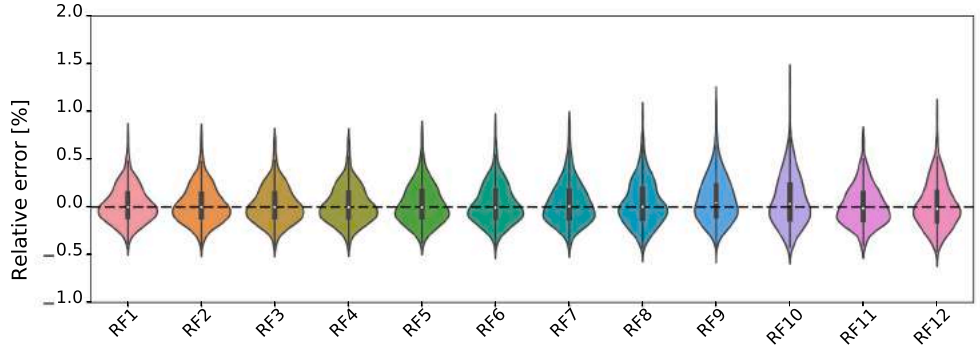

(b) RF models

Fig. 12. Violin plots of the ET_a relative errors in predictions obtained using (a) MLP models and (b) RF models.

tions, can be a useful solution to improve the estimation of effective crop water requirements, with the aim to choose the best irrigation strategies for sustainable water management of productive ecosystems. In this context, the availability of continuous daily actual evapotranspiration time series is essential to implement, at local and regional scale, agro-hydrological models to support policy decisions and to better optimize agricultural practices.

Declaration of Competing Interest

The authors declare that they have no known competing financial interests or personal relationships that could have appeared to influence the work reported in this paper.

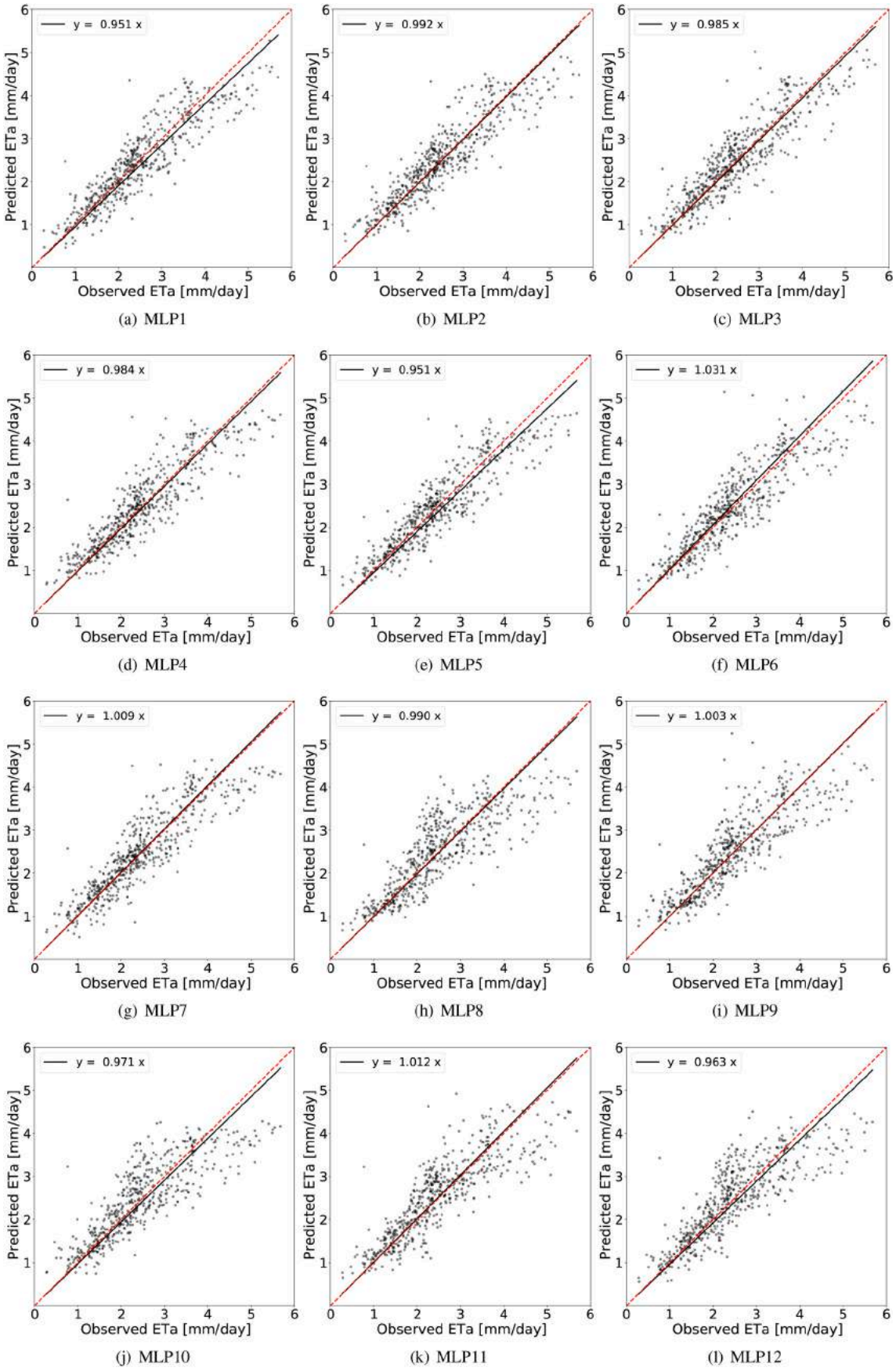

Fig. 13. Comparison of predicted daily ET_a values by MLP methods with observed values for the testing subsets.

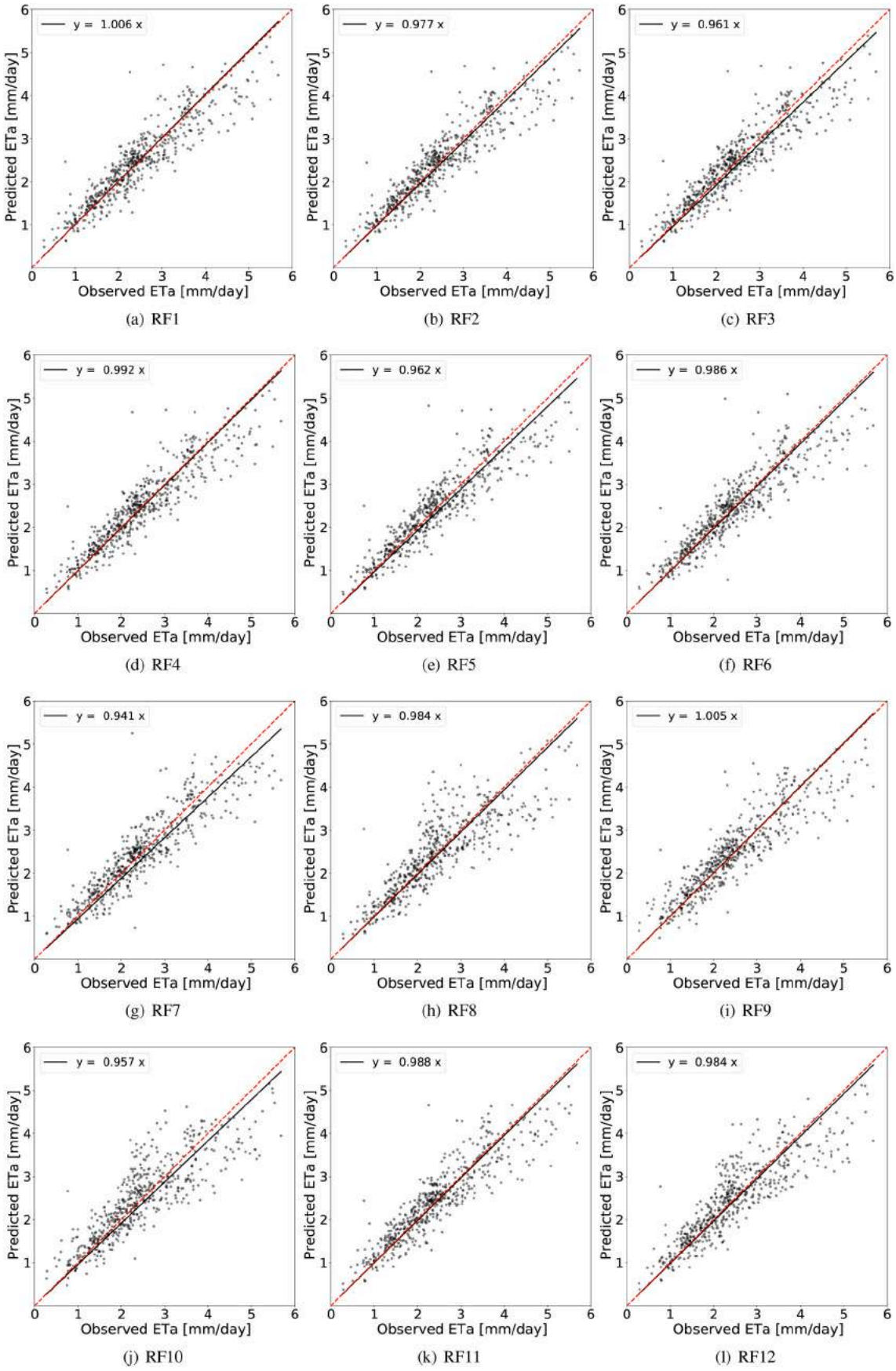

Fig. 14. Comparison of predicted daily ET_a values by RF methods with observed values for the testing subsets.

Data availability

The data that has been used is confidential.

Acknowledgments

The authors would like to express their profound gratitude to Prof. Giuseppe Provenzano (who sadly passed away in December 2022) for his significant contributions to the initial draft of this article, as well as for fostering extraordinary human and professional relationships.

This work was partially supported by the European Union under the Italian National Recovery and Resilience Plan (NRRP) of NextGenerationEU, partnership on "Telecommunications of the Future" (PE00000001 - program "RESTART") and by the Italian "Ministero dell'Istruzione, dell'Università e della Ricerca", in the project "INtegrated Computer modeling and monitoring for Irrigation Planning in ITaly – INCIPIT" (PRIN 2017).

References

Abrishami, N., Sepaskhah, A.R., Shahrokhnia, M.H., 2019. Estimating wheat and maize daily evapotranspiration using artificial neural network. Theoret. Appl. Climatol. 135 (3), 945–958.

Aghajanloo, M.-B., Sabziparvar, A.-A., Hosseinzadeh Talaee, P., 2013. Artificial neural network–genetic algorithm for estimation of crop evapotranspiration in a semi-arid region of iran. Neural Comput. Appl. 23 (5), 1387–1393.

Alkaeed, O., Flores, C., Jinno, K., Tsutsumi, A., 2006. Comparison of several reference evapotranspiration methods for itoshima peninsula area, fukuoka, japan. Mem. Fac. Eng. Kyushu Univ. 66 (1).

Allen, R.G., Pereira, L.S., Raes, D., Smith, M., et al., 1998. Fao irrigation and drainage paper no. 56. Food and Agriculture Organization of the United Nations, Rome, e156, 56 (97).

Bastiaanssen, W.G., Menenti, M., Feddes, R., Holtslag, A., 1998. A remote sensing surface energy balance algorithm for land (sebal). 1. formulation. J. Hydrol. 212, 198–212.

Breiman, L., 1996. Bagging predictors. Mach. Learn. 24 (2), 123–140.

Breiman, L., 2001. Random forests. Mach. Learn. 45 (1), 5–32.

Castel, J., 2000. Water use of developing citrus canopies in valencia, spain. In: Proceeding International Society Citriculture, IX Congress. pp. 223–226.

Consoli, S., Stagno, F., Roccuzzo, G., Cirelli, G., Intrigliolo, F., 2014. Sustainable management of limited water resources in a young orange orchard. Agric. Water Manag. 132, 60–68.

El Hari, A., Chaik, M., Lekouch, N., Sedki, A., Lahrouni, A., 2010. Water needs in citrus fruit in a dry region of morocco. J. Agric. Environ. Int. Dev. (JAEID) 104 (3/4), 91–99.

Elbeltagi, A., Deng, J., Wang, K., Malik, A., Maroufpoor, S., 2020. Modeling long-term dynamics of crop evapotranspiration using deep learning in a semi-arid environment. Agric. Water Manag. 241, 106334.

Er-Raki, S., Chehbouni, A., Guemouria, N., Ezzahar, J., Khabba, S., Boulet, G., Hanich, L., 2009. Citrus orchard evapotranspiration: comparison between eddy covariance measurements and the fao-56 approach estimates. Plant Biosyst. 143 (1), 201–208.

Gangopadhyay, S., Saha, A., Pal, S.C., Banerjee, R., Batabyal, S., Das, N., Ghosh, P.B., Mondal, A., Mandal, S., 2023. A new methodological approach to the establishment of sustainable agricultural ecology in drought vulnerable areas of eastern india. Ecol. Inform., 102013

Gao, B.-C., 1996. Ndwi—a normalized difference water index for remote sensing of vegetation liquid water from space. Remote Sens. Environ. 58 (3), 257–266.

Girardello, M., Griggio, M., Whittingham, M.J., Rushton, S.P., 2010. Models of climate associations and distributions of amphibians in italy. Ecol. Res. 25, 103–111.

Git Repository, 2023. Machine learning models to predict daily actual evapotranspiration of citrus orchards. Accessed: 15/03/2023.https://github.com/fedesss98/ml-to-eta-of-citrus-orchards.git.

González-Altozano, P.e.a., 2000. Regulated deficit irrigation in 'clementina de nules' citrus trees. ii: Vegetative growth. J. Hortic. Sci. Biotechnol. 75 (4), 388–392.

Granata, F., 2019. Evapotranspiration evaluation models based on machine learning algorithms—a comparative study. Agric. Water Manag. 217, 303–315.

Granata, F., Gargano, R., de Marinis, G., 2020. Artificial intelligence based approaches to evaluate actual evapotranspiration in wetlands. Sci. Total Environ. 703, 135653.

Han, X., Wei, Z., Zhang, B., Li, Y., Du, T., Chen, H., 2021. Crop evapotranspiration prediction by considering dynamic change of crop coefficient and the precipitation effect in back-propagation neural network model. J. Hydrol. 596, 126104.

Hao, Y., Baik, J., Tran, H., Choi, M., 2022. Quantification of the effect of hydrological drivers on actual evapotranspiration using the bayesian model averaging approach for various landscapes over northeast asia. J. Hydrol. 607, 127543.

Hashemi, M., et al., 2020. Evaluation of artificial neural network and penman–monteith equation for the prediction of barley standard evapotranspiration in a semi-arid region. Theoret. Appl. Climatol. 139 (1), 275–285.

Ho, T.K., 1998. The random subspace method for constructing decision forests. IEEE Trans. Pattern Anal. Mach. Intell. 20 (8), 832–844.

Ippolito, M., De Caro, D., Ciraolo, G., Minacapilli, M., Provenzano, G., 2022. Estimating crop coefficients and actual evapotranspiration in citrus orchards with sporadic cover weeds based on ground and remote sensing data. Irrig. Sci. 1–18.

Izadifar, Z., et al., 2010. Prediction of hourly actual evapotranspiration using neural networks, genetic programming, and statistical models. Hydrol. Process. 24 (23), 3413–3425.

Jing, W., Yaseen, Z.M., Shahid, S., Saggi, M.K., Tao, H., Kisi, O., Salih, S.Q., Al-Ansari, N., Chau, K.-W., 2019. Implementation of evolutionary computing models for reference evapotranspiration modeling: short review, assessment and possible future research directions. Eng. Appl. Comput. Fluid Mech. 13 (1), 811–823.

Kadiyala, A., Kumar, A., 2018. Applications of python to evaluate the performance of decision tree-based boosting algorithms. Environ. Progress Sustain. Energy 37 (2), 618–623.

Kelley, J., et al., 2019. Using neural networks to estimate site-specific crop evapotranspiration with low-cost sensors. Agronomy 9 (2), 108.

Kingma, D.P., Ba, J., 2014. Adam: A method for stochastic optimization. arXiv preprint arXiv:1412.6980.

Kottek, M., Grieser, J., Beck, C., Rudolf, B., Rubel, F., 2006. World map of the köppen-geiger climate classification updated. Meteorol. Z. 15 (3), 259–263.

Krishnashetty, P.H., Balasangameshwara, J., Sreeman, S., Desai, S., Kantharaju, A.B., 2021. Cognitive computing models for estimation of reference evapotranspiration: A review. Cognit. Syst. Res. 70, 109–116.

Kustas, W.P., Prueger, J.H., Humes, K.S., Starks, P.J., 1999. Estimation of surface heat fluxes at field scale using surface layer versus mixed-layer atmospheric variables with radiometric temperature observations. J. Appl. Meteorol. 38 (2), 224–238.

Lap, B.Q., Du Nguyen, H., Hang, P.T., Phi, N.Q., Hoang, V.T., Linh, P.G., Hang, B.T.T., et al., 2023. Predicting water quality index (wqi) by feature selection and machine learning: A case study of an kim hai irrigation system. Ecol. Inform., 101991

Lei, H., Yang, D., 2014. Combining the crop coefficient of winter wheat and summer maize with a remotely sensed vegetation index for estimating evapotranspiration in the north china plain. J. Hydrol. Eng. 19 (1), 243–251.

Liu, J., Meng, X., Ma, Y., Liu, X., 2020. Introduce canopy temperature to evaluate actual evapotranspiration of green peppers using optimized enn models. J. Hydrol. 590, 125437.

Lukangu, G., Savage, M.J., Johnston, M.A., 1999. Use of sub-hourly soil water content measured with a frequency-domain reflectometer to schedule irrigation of cabbages. Irrig. Sci. 19 (1), 7–13.

Main-Knorn, M., Pflug, B., Louis, J., Debaecker, V., Müller-Wilm, U., Gascon, F., 2017. Sen2cor for sentinel-2. In: Image and Signal Processing for Remote Sensing XXIII, vol. 10427. SPIE, pp. 37–48.

Manca, G., 2003. Analisi dei flussi di carbonio di una cronosequenza di cerro (quercus cerris l.) dell'italia centrale attraverso la tecnica della correlazione turbolenta. PhD Dissertation Thesis. University of Tuscia, Viterbo, p. 225.

MAPA, 2019. Encuesta sobre superficies y rendimientos de cultivos en españa. Subsecretaría de Agricultura, Pesca y Alimentación, Ministerio de Agricultura, Pesca y Alimentación, Madrid, España.

Masseroni, D., Corbari, C., Mancini, M., 2014. Limitations and improvements of the energy balance closure with reference to experimental data measured over a maize field. Atmósfera 27 (4), 335–352.

Mosre, J., et al., 2021. Actual evapotranspiration estimates in arid cold regions using machine learning algorithms with in situ and remote sensing data. Water 13 (6), 870.

Norman, J.M., Kustas, W.P., Humes, K.S., 1995. Source approach for estimating soil and vegetation energy fluxes in observations of directional radiometric surface temperature. Agric. For. Meteorol. 77 (3–4), 263–293.

Pedregosa, et al., 2011. Scikit-learn: Machine learning in Python. J. Mach. Learn. Res. 12, 2825–2830.

Pereira, L., Paredes, P., Jovanovic, N., 2020. Soil water balance models for determining crop water and irrigation requirements and irrigation scheduling focusing on the fao56 method and the dual kc approach. Agric. Water Manag. 241, 106357.

Piccioni, F., Casenave, C., Baragatti, M., Cloez, B., Vinçon-Leite, B., 2022. Calibration of a complex hydro-ecological model through approximate bayesian computation and random forest combined with sensitivity analysis. Ecol. Inform. 71, 101764. URL: https://www.sciencedirect.com/science/article/pii/S157495412200214X.

Pierantozzi, P., Torres, M., Bodoira, R., Maestri, D., 2013. Water relations, biochemical – physiological and yield responses of olive trees (olea europaea l. cvs. arbequina and manzanilla) under drought stress during the pre-flowering and flowering period. Agric. Water Manag. 125, 13–25. URL:https://www.sciencedirect.com/science/article/pii/S0378377413000942.

Pôças, I., Calera, A., Campos, I., Cunha, M., 2020. Remote sensing for estimating and mapping single and basal crop coefficientes: A review on spectral vegetation indices approaches. Agric. Water Manag. 233, 106081.

Prueger, J., Hatfield, J., Parkin, T., Kustas, W., Hipps, L., Neale, C., MacPherson, J., Eichinger, W., Cooper, D., 2005. Tower and aircraft eddy covariance measurements of water vapor, energy, and carbon dioxide fluxes during smacex. J. Hydrometeorol. 6 (6), 954–960.

Puig-Sirera, À., Provenzano, G., González-Altozano, P., Intrigliolo, D.S., Rallo, G., 2021. Irrigation water saving strategies in citrus orchards: Analysis of the combined effects of timing and severity of soil water deficit. Agric. Water Manag. 248, 106773.

Reyes Rojas, L.A., Moletto-Lobos, I., Corradini, F., Mattar, C., Fuster, R., Escobar-Avaria, C., 2021. Determining actual evapotranspiration based on machine learning and sinusoidal approaches applied to thermal high-resolution remote sensing imagery in a semi-arid ecosystem. Remote Sens. 13 (20), 4105.

Rallo, G., González-Altozano, P., Manzano-Juárez, J., Provenzano, G., 2017. Using field measurements and fao-56 model to assess the eco-physiological response of citrus orchards under regulated deficit irrigation. Agric. Water Manag. 180, 136–147.

Rallo, G., Paço, T., Paredes, P., Puig-Sirera, À., Massai, R., Provenzano, G., Pereira, L., 2021. Updated single and dual crop coefficients for tree and vine fruit crops. Agric. Water Manag. 250, 106645.

Ranghetti, L., Boschetti, M., Nutini, F., Busetto, L., 2020. "sen2r": An R toolbox for automatically downloading and preprocessing sentinel-2 satellite data. Comput. Geosci. 139, 104473 https://doi.org/10.1016/j.cageo.2020.104473. URL:https://sen2r.ranghetti.info.

Ravindran, S.M., Bhaskaran, S.K.M., Ambat, S.K.N., 2021. A deep neural network architecture to model reference evapotranspiration using a single input meteorological parameter. Environ. Process. 8 (4), 1567–1599. https://doi.org/10.1007/s40710-021-00543-x.

Richman, M.B., Trafalis, T.B., Adrianto, I., 2009. Missing data imputation through machine learning algorithms. In: Artificial intelligence methods in the environmental sciences. Springer, pp. 153–169.

Rouse, J., Haas, R., Schell, J., Deering, D., 1974. Monitoring vegetation systems in the great plains with erts. In: Proceedings of the third earth resources technology satellite-1 symposium. NASA SP-351, pp. 301–317.

Schrader, F., Durner, W., Fank, J., Gebler, S., Pütz, T., Hannes, M., Wollschläger, U., 2013. Estimating precipitation and actual evapotranspiration from precision lysimeter measurements. Proc. Environ. Sci. 19, 543–552.

Sowmya, M., Kumar, M.S., Ambat, S.K., 2020. Comparison of deep neural networks for reference evapotranspiration prediction using minimal meteorological data. In: 2020 advanced computing and communication Technologies for High Performance Applications (ACCTHPA). IEEE, pp. 27–33.

Srinet, R., Nandy, S., Patel, N., 2019. Estimating leaf area index and light extinction coefficient using random forest regression algorithm in a tropical moist deciduous forest, india. Ecol. Inform. 52, 94–102.

Stagno, F., Intrigliolo, F., Consoli, S., Continella, A., Roccuzzo, G., 2015. Response of orange trees to deficit irrigation strategies: Effects on plant nutrition, yield, and fruit quality. J. Irrig. Drain. Eng. 141 (10), 04015014.

Talib, A., Desai, A.R., Huang, J., Griffis, T.J., Reed, D.E., Chen, J., 2021. Evaluation of prediction and forecasting models for evapotranspiration of agricultural lands in the midwest us. J. Hydrol. 600, 126579.

Tang, D., Feng, Y., Gong, D., Hao, W., Cui, N., 2018. Evaluation of artificial intelligence models for actual crop evapotranspiration modeling in mulched and non-mulched maize croplands. Comput. Electron. Agric. 152, 375–384.

Thirukumaran, S., Sumathi, A., 2012. Missing value imputation techniques depth survey and an imputation algorithm to improve the efficiency of imputation. In: 2012 Fourth International Conference on Advanced Computing (ICoAC). IEEE, pp. 1–5.

Toosi, A., Javan, F.D., Samadzadegan, F., Mehravar, S., Kurban, A., Azadi, H., 2022. Citrus orchard mapping in juybar, iran: Analysis of ndvi time series and feature fusion of multi-source satellite imageries. Ecol. Inform. 70, 101733.

Troyanskaya, O., Cantor, M., Sherlock, G., Brown, P., Hastie, T., Tibshirani, R., Botstein, D., Altman, R.B., 2001. Missing value estimation methods for dna microarrays. Bioinformatics 17 (6), 520–525.

Volschenk, T., 2020. Water use and irrigation management of pomegranate trees - a review. Agric. Water Manag. 241, 106375. URL:https://www.sciencedirect.com/science/article/pii/S0378377420303231.

Walls, S., Binns, A.D., Levison, J., MacRitchie, S., 2020. Prediction of actual evapotranspiration by artificial neural network models using data from a bowen ratio energy balance station. Neural Comput. Appl. 32 (17), 14001–14018.

Wang, K., Liang, S., 2008. An improved method for estimating global evapotranspiration based on satellite determination of surface net radiation, vegetation index, temperature, and soil moisture. J. Hydrometeorol. 9 (4), 712–727.

Wang, X., Gao, B., Wang, X.-S., 2022. Investigating the ability of deep learning on actual evapotranspiration estimation in the scarcely observed region. J. Hydrol. 607, 127506.

Wang, X., Zhong, L., Ma, Y., Fu, Y., Han, C., Li, P., Wang, Z., Qi, Y., 2023. Estimation of hourly actual evapotranspiration over the tibetan plateau from multi-source data. Atmos. Res. 281, 106475.

WWDR, 2021. The united nations world water development report 2021: valuing water. UNESCO World Water Assessment Programme. URL:https://unesdoc.unesco.org/ark:/48223/pf0000375724.

Yamaç, S.S., 2021. Artificial intelligence methods reliably predict crop evapotranspiration with different combinations of meteorological data for sugar beet in a semiarid area. Agric. Water Manag. 254, 106968.

Yamaç, S.S., et al., 2020. Estimation of daily potato crop evapotranspiration using three different machine learning algorithms and four scenarios of available meteorological data. Agric. Water Manag. 228, 105875.

Yao, W., Han, M., Xu, S., 2010. Estimating the regional evapotranspiration in zhalong wetland with the two-source energy balance (tseb) model and landsat7/etm+ images. Ecol. Inform. 5 (5), 348–358.

Zhang, C., Luo, G., Hellwich, O., Chen, C., Zhang, W., Xie, M., He, H., Shi, H., Wang, Y., 2021. A framework for estimating actual evapotranspiration at weather stations without flux observations by combining data from modis and flux towers through a machine learning approach. J. Hydrol. 603, 127047.

Zhang, L., Wang, R., Zhang, C., Wang, S., Xu, T., 2016. Intelligent irrigation strategy based on regulated deficit theory and fuzzy control for rice in cold region. Trans. Chin. Soc. Agric. Eng. 32 (13), 52–58.